International Journal of Solids and Structures 144–145 (2018) 100–122

Contents lists available at ScienceDirect

International Journal of Solids and Structures

journal homepage: www.elsevier.com/locate/ijsolstr

On G_c, J_c and the characterisation of the mode-I fracture resistance in delamination or adhesive debonding

Leo Škec[a,*], Giulio Alfano[a], Gordan Jelenić[b]

[a] Department of Mechanical and Aerospace Engineering, Brunel University London, Kingston Lane, Uxbridge UB8 3PH, UK
[b] Faculty of Civil Engineering, University of Rijeka, Radmile Matejčić 3, Rijeka 51000, Croatia

ARTICLE INFO

Article history:
Received 28 November 2017
Revised 15 February 2018
Available online 27 April 2018

Keywords:
DCB test
Mode-I delamination
Data-reduction schemes
Fracture toughness
Crack length measurement
Cohesive zone models

ABSTRACT

We focus on the mode-I quasi-static crack propagation in adhesive joints or composite laminates, where inelastic behaviour is due to damage on a relatively thin interface that can be effectively modelled with a cohesive-zone model (CZM). We studied the difference between the critical energy release rate, G_c, introduced in linear elastic fracture mechanics (LEFM), and the work of separation, Ω, i.e. the area under the traction-separation law of the CZM. This difference is given by the derivative, with respect to the crack length, of the energy dissipated ahead of the crack tip per unit of specimen width. For a steady-state crack propagation, in which that energy remains constant as the crack tip advances, this derivative vanishes and $\Omega = G_c$. Thus, the difference between Ω and G_c depends on how far from steady-state the process is, and not on the size of the damage zone, unlike what is stated elsewhere in the literature. Therefore, even for very ductile interfaces, $G_c = \Omega$ for a double cantilever beam (DCB) loaded with moments and their difference is extremely small for a DCB loaded with forces. We also show that the proof that the critical value of the J integral, J_c, is equal to the nonlinear energy release rate is not valid for a non-homogeneous material. To compute G_c for a DCB, we use a method based on the introduction of an equivalent crack length, a_{eq}, where the solution is a product of a closed-form part, which does not require the measurement of the actual crack length, and of a corrective factor where the knowledge of the actual crack length is required. However, we also show that this factor is close to unity and therefore has a very small effect on G_c.

1. Introduction

In the last few years, the validity of data-reduction methods derived from linear elastic fracture mechanics (LEFM), for the experimental determination of the fracture resistance during adhesive joint debonding or composite delamination in presence of 'large-scale' fracture processes, has been seriously questioned (Sarrado et al., 2016; Sørensen and Jacobsen, 2003; Zhao et al., 2016; Campilho et al., 2015; Dimitri et al., 2017). Although not all authors are so clear in stating that "LEFM is not applicable to those specimens containing large fracture process zone around the delamination front" (Zhao et al., 2016), there is a general consensus that, in presence of large process zones, J-integral theory provides a more accurate framework to determine the fracture resistance. In terms of real-life engineering applications, these conclusions are very significant because all the current methods available in ASTM, BS ISO and BS EN standards are based on LEFM.

It has also been noted that a very accurate characterisation of the fracture process for the aforementioned types of problems cannot be obtained using a one-parameter fracture-mechanics theory and, therefore, the richer modelling framework of cohesive-zone models (CZMs) should be used instead (Sørensen and Jacobsen, 2003). With a CZM, the interface response is defined by a nonlinear relationship between the interface traction σ and the relative displacement, δ, between the top and bottom sides of the interface, also indicated as 'traction-separation' law. In this article we focus on mode-I crack propagation, whereby σ and δ represent the direct tensile stress and the mode-I (opening) relative displacement, respectively. A number of authors have exploited a relation which provides the traction separation law as the derivative of the J integral, J, with respect to the relative displacement at the crack tip, δ_{CT}. Based on this relationship, one can also show that the critical value of the J integral leading to crack propagation, J_c, must be

* Corresponding author.
E-mail addresses: leo.skec@brunel.ac.uk (L. Škec), giulio.alfano@brunel.ac.uk (G. Alfano), gordan.jelenic@uniri.hr (G. Jelenić).

https://doi.org/10.1016/j.ijsolstr.2018.04.020

equal to the area, Ω, under the traction separation curve, that is the 'work of separation'.

One aspect that does not seem to be clearly addressed in the literature is how to assess the accuracy of a certain method used to determine the fracture resistance. In other words, what do we mean by 'fracture resistance'? Assuming that a single energy value can be taken to characterise the fracture resistance of an interface, two values can be considered: one is the work of separation, Ω, and a second value is the energy released (i.e. dissipated) per unit of new crack area. The latter is called the critical energy release rate, and denoted by G_c in LEFM. For the more general cases considered here, which include nonlinear behaviour due to progressive damage at the interface, the critical energy release rate can be still computed and will be denoted by G_c, too. In the authors' opinion, which one of these values is the most appropriate to characterise the fracture resistance generally depends on the problem considered, the aims of the investigation and the methods of analysis used. One could argue that $J_c = \Omega$ and therefore these two parameters are equivalent. However, we will show in this paper that, for a non-flat R-curve (i.e. the fracture resistance varying with the increase of the crack), $J_c \neq \Omega$ if the R-curve is modelled by using a CZM with input parameters which vary along the interface.

Therefore, to characterise fracture resistance by a single energy value, we have three candidates, Ω, G_c and J_c and, in general, $G_c \neq J_c$, $G_c \neq \Omega$ and $J_c \neq \Omega$.

In the general case, Ω is the only parameter that can be considered as an interface property and, ultimately, the integral of Ω over the entire interface provides the energy dissipated during crack propagation when the entire interface has failed. Therefore, for the purpose of this study, we will assess the accuracy of a data-reduction method by evaluating how closely it predicts Ω.

The data-reduction methods in the current standards, as well as those proposed in the literature based on analytical formulae, are all ways to evaluate either G_c or J_c. Ripling et al. (1964, 1971) in the mid 1960's and early 1970's proposed methods for measuring the mode-I value of G_c in adhesive joints. Based on these studies, the first American standard for determining fracture resistance in adhesive joints was introduced in 1974 (current version is ASTM D3433-99, 2012). A British Standard, which is based on the work by Blackman and Kinloch (1997) and their co-workers from Imperial College London in the 1990's, was first published in 2001 (BS ISO 15024:2001, 2001). Up to this day, many different standard procedures for determining G_c in adhesive joints and composite laminates have been developed for different materials, specimens, geometries, fracture modes etc. The double cantilever beam (DCB) specimen is the most commonly used specimen in all the standards due to its simple geometry and a rather simple testing procedure used for mode I delamination or debonding. Therefore, although other tests exist, in this paper we will focus on the DCB test only.

A common approach for determining G_c in all standards is to use simple analytical formulae based on linear beam theories (Euler–Bernoulli or Timoshenko). In this approach, we assume that the DCB is composed of one part where complete debonding between the arms has occurred and the other part where the arms are still bonded together and undeformed. This is equivalent to assuming that the DCB arms are clamped at the crack tip. However, as is well known, due to the actual rotation of the arms at the crack tip and nonlinear effects that take place around the crack tip (e.g. damage, plasticity), the cantilever beam deflection formulae are not accurate if they are written in terms of the actual crack length. Instead, they can be made relatively accurate if the actual crack length is appropriately 'corrected'. In fact, in BS ISO 25217:2009 (2009), a data reduction scheme called 'corrected beam theory' (CBT) features corrections of the actual measured crack length, whereas in 'experimental compliance method' (ECM) (BS ISO 25217:2009, 2009) the value of G_c is corrected by a factor obtained from the measured compliance. In ASTM D5528 (2013) and BS ISO 15024:2001 (2001) for carbon fibre reinfored polymers (CFRP), an additional method, called 'modified compliance calibration' (MCC) method, quite similar to CBT is introduced. In ASTM D5528 (2013) it is mentioned that a round-robin testing performed by ASTM showed that the values of G_c determined using CBT, ECM and MCC differed no more than 3.1%. However, CBT, which in ASTM is called 'modified beam theory' (MBT), is recommended as it yielded the most conservative values of G_c for 80% of the specimens tested (ASTM D5528, 2013).

All the formulae used in the standards, besides requiring the measurement of the applied force and cross-head displacement, also require the measurement of the crack length. Since this is usually done optically (typically by means of a travelling microscope or a high-resolution camera), determining the exact position of the crack tip is extremely difficult and time-consuming, and it can introduce significant uncertainty in the determination of G_c.

Many authors have so far recognised the difficulty and inconvenience of measuring the crack length in DCB experiments (Lopes et al., 2016; de Moura et al., 2008; Alfano et al., 2011; Tamuz et al., 2003) and suggested alternative approaches. Their idea is that cantilever beam deflection formulae can actually be re-used to express the crack length in terms of the applied force and the cross-head displacement, F and v. However, in most of the above cited articles, with few exceptions (e.g. 'compliance-based beam method' (CBBM) by de Moura et al., 2008), it is not noted that the crack length so determined is not the actual one, but really an 'equivalent crack length', a_{eq}, which can be defined as the crack length that makes the actual cantilever beam formulae valid. Using Euler–Bernoulli beam theory, determining a_{eq} is straightforward and many authors (Tamuz et al., 2003; Alfano et al., 2011; Biel and Stigh, 2007 to name just a few) use this approach. However, they do not recognise the important difference between a and a_{eq}, and use a for what should actually be a_{eq}. For Timoshenko beam theory, computing a_{eq} is less straightforward as a_{eq} is a solution of a cubic equation. This may be computed numerically (see de Moura et al., 2008), but a closed-form solution can also be found, as we show later in this paper.

What is certainly not recognised in any of these alternative approaches is that, during quasi-static crack propagation, G_c is the derivative of the total potential energy with respect to the actual crack length, a, not with respect to a_{eq}. This normally results in an error in the determination of G_c which should be taken into account in an investigation on the accuracy of these methods, such as the one presented in this paper. In addition, the difference $a - a_{eq}$ is generally not constant, and therefore a constant correction term such as the one used in CBT (BS ISO 25217:2009, 2009) may result in an error in the evaluation of G_c, too.

As a summary, from the practical point of view of an engineer who intends to characterise the mode-I debonding or delamination resistance in adhesive joints and composite laminates, the following issues remain open:

- A large number of standards have been released for what is basically the same problem, with significant differences in the testing procedures and data reduction methods, which makes it unclear what the best method is.
- All the approved standards require the measurement of the crack length, which makes them impractical, although a number of authors have proposed methods which do not require such measurement.
- The aforementioned methods, which do not require the crack length measurement, do not take into account the difference between the actual and the equivalent crack length, a and a_{eq}. This can result in errors of an amount that is as yet unknown.

- In the case of ductile interfaces the size of the part of the specimens where nonlinear dissipative phenomena occur is relatively large, compared to the specimen dimensions. According to many authors, this violates one of the main assumptions in LEFM and therefore can potentially lead to very significant errors if LEFM is used, which however are not quantified by the standards. In these cases, according to most authors, the use of J_c instead of G_c as the driving energy for crack propagation produces more accurate predictions of the fracture resistance.
- If one parameter is considered not sufficient to characterise the interface response with sufficient accuracy and a CZM is used instead, the available methods provide a more or less accurate approximation of the area under the traction-separation curve of the CZM. According to many authors, the use of the J integral also allows one to determine the entire law experimentally. However, if the stress at the crack tip, σ_{CT}, is equal to $\mathrm{d}J/\mathrm{d}\delta_{CT}$, the latter should be zero when $\sigma_{CT} = 0$. However, in the case of a non-flat R-curve one should also expect $\mathrm{d}J/\mathrm{d}\delta_{CT} \neq 0$ when $\sigma_{CT} = 0$, as at this point $J = J_c$ and represents the fracture resistance, varying with further increase in δ_{CT}. This raises concerns regarding the range of validity of the formulation. Also, the procedure requires the precise evaluation of the crack tip displacement, which is again difficult, expensive and time consuming. Simpler ways to evaluate the CZM parameters do not seem to be available.

This article aims to address all the above open questions. In Section 2 we revisit some fundamental concepts behind LEFM, nonlinear fracture mechanics and how they relate to the predictions of the 'work of separation', Ω, to be used as key input parameter for a CZM on the interface. To this end, the derivation of Griffith's criterion is revisited and the importance of whether the dissipation process advances in a steady-state manner with the crack tip is highlighted. We determine the relationships between G_c, J_c and Ω which clarify the actual range of validity of LEFM and of J-integral theory.

In Section 3, we take into account that $a_{eq} \neq a$ and derive consistent formulae for G_c for DCB specimens with prescribed displacement or rotations valid for Euler–Bernoulli and Timoshenko beam theories, which do not require the measurement of the crack length.

The accuracy of the formulae from BS ISO 25217:2009 and the formulae we propose is assessed in Sections 4 and 5 for the case in which Ω is constant on the interface (flat R-curve), using a very similar approach to the one used by Biel and Stigh (2007). In this approach, numerical models, which allow for nonlinear effects at the interface, are used as 'virtual experiments' to create input data for analytical formulae (namely *a, F* and *v*).

In Section 4.4 we analyse the case of a non-flat R curve. For this case, if the decohesion process is modelled with a CZM, its input properties must be taken as variable along the interface. Therefore, we present a comparison of the R-curves calculated using the methods presented in Section 3, including J-integral theory. The peculiar aspects of the response related to the non-flat R-curve are explained and discussed.

Finally, in Section 6 conclusions are drawn, first in terms of direct impact on real-life engineering applications and then in terms of fundamental novelties presented in this work.

2. Relationships between G_c, J_c and Ω

In this section we will first review some fundamental concepts underpinning the theories of linear elastic and nonlinear inelastic fracture mechanics. For the latter, we will focus on the important case in which the mechanical response can be effectively modelled by assuming that rate-independent damage (with no plasticity) occurs within a negligibly thin planar interface, whereas the behaviour of the remaining parts of the structure is well approximated by linear elastic behaviour.

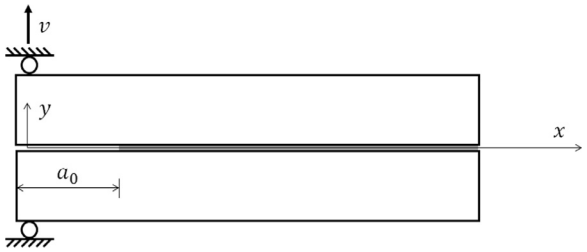

Fig. 1. Mode-I crack propagation under displacement control.

Let us consider the case of a specimen that can be effectively modelled as a 2D solid, in quasi-static isothermal conditions, pinned in two points, subject to a monotonically increasing prescribed (opening) displacement, *v*, on one of its pinned ends as shown in Fig. 1. Furthermore, an initial flat crack of length a_0, is assumed to be present, which is in a plane of geometric, material and loading symmetry of the body so that crack propagation, once started, continues in mode I.

Although, for the sake of simplicity, the treatment in this section considers a prescribed displacement, the results are indeed valid for any type of prescribed kinematics on some part of the body, including in particular the case of prescribed rotations, that will be considered in Section 3.

2.1. Derivation of LEFM Griffith's criterion from the first principle of thermodynamics

For the developments presented later in Sections 2.2–2.4 it is useful to show how Griffith's crack propagation criterion can be derived from the first principle of thermodynamics.

If material behaviour is linear elastic everywhere (except at the crack tip, as discussed below) the total potential energy can be expressed as a function Π of the prescribed displacement, *v*, and the crack length, *a*, which are both functions of time *t*. Hence, as a function of time, the total potential energy can be expressed as the compound function

$$\hat{\Pi}(t) = \Pi(a(t), v(t)). \tag{1}$$

The rate of change of $\hat{\Pi}$ must be equal to the mechanical power $\dot{W}$ transmitted to the solid minus the power dissipated $\dot{\mathcal{D}}$:

$$\dot{\hat{\Pi}} = \dot{W} - \dot{\mathcal{D}}, \tag{2}$$

where the dot represents the derivative with respect to *t*. Denoting by *F* the reaction force where *v* is prescribed, $\dot{W}$ is given by

$$\dot{W} = F\,\dot{v}. \tag{3}$$

Differentiating (1) and replacing in (2), using (3) one has

$$\dot{\hat{\Pi}} = \frac{\partial \Pi}{\partial v}\,\dot{v} + \frac{\partial \Pi}{\partial a}\,\dot{a} = F\,\dot{v} - \dot{\mathcal{D}}. \tag{4}$$

However, since

$$\frac{\partial \Pi}{\partial v} = F, \tag{5}$$

this leads to

$$\frac{\partial \Pi}{\partial a}\,\dot{a} = -\dot{\mathcal{D}}. \tag{6}$$

Introducing the critical energy release rate, G_c, by setting

$$\dot{a} > 0 \qquad \Rightarrow \qquad G_c = \frac{\dot{\mathcal{D}}}{b\dot{a}}, \tag{7}$$

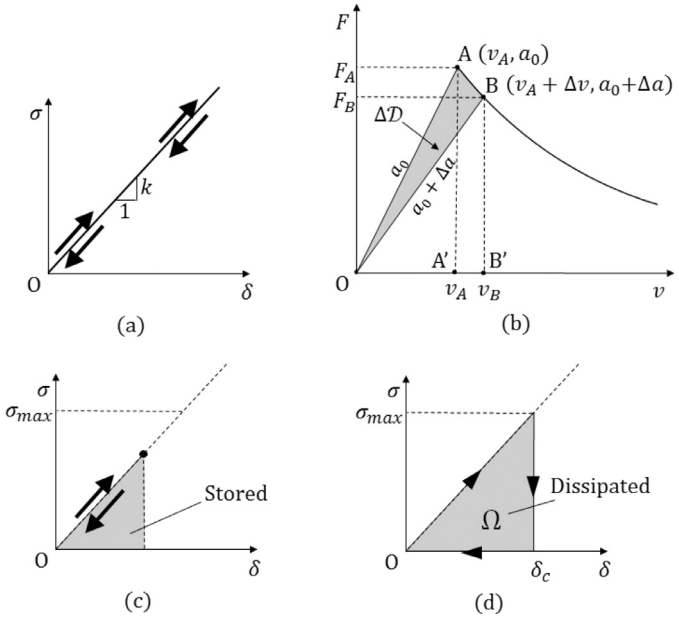

Fig. 2. Linear elastic interface behaviour (a) linear elastic law (no material failure explicitly included) and (b) the associated structural response; equivalent CZM law for (c) an undamaged point and (d) a damaged one.

and replacing into (6), Griffth's criterion for crack propagation in quasi-static conditions is obtained:

$$\dot{a} > 0 \qquad \Rightarrow \qquad -\frac{1}{b}\frac{\partial \Pi}{\partial a} = G_c. \tag{8}$$

By expressing the total dissipation as a function $\hat{\mathcal{D}}$ of the crack length a, so that $\mathcal{D}(t) = \hat{\mathcal{D}}(a(t))$, one has

$$\dot{a} > 0 \qquad \Rightarrow \qquad G_c = \frac{\dot{\mathcal{D}}}{b\dot{a}} = \frac{1}{b}\frac{\mathrm{d}\hat{\mathcal{D}}}{\mathrm{d}a}, \tag{9}$$

which emphasises the physical meaning of G_c as the energy dissipated per unit of new crack area formed.

Classic fracture mechanics can also be formulated within the theory of thermodynamics with internal variables by interpreting the crack length, a, as an internal variable, so that $\Pi(a(t), v(t))$ represents the free energy of the system at time t. In this way, Eq. (2) can be written in the form of Clausius–Duhem inequality:

$$\dot{\mathcal{D}} = \dot{W} - \dot{\Pi} = \left(F - \frac{\partial \Pi}{\partial v}\right)\dot{v} - \frac{\partial \Pi}{\partial a}\dot{a} \geq 0 \qquad \text{for any } \dot{v} \text{ and } \dot{a} \tag{10}$$

Using standard thermodynamic arguments (Lemaitre and Chaboche, 1990), Eq. (5) is then obtained. Furthermore, $-\partial\Pi/\partial a$ is now the thermodynamic variable that is work-conjugate to a. Since $\partial\Pi/\partial a \leq 0$, it must also be $\dot{a} \geq 0$ for the dissipated power, $\dot{\mathcal{D}}$, to be non-negative. Introducing the energy release rate, G:

$$G = -\frac{1}{b}\frac{\partial \Pi}{\partial a} \qquad \text{(whether or not } \dot{a} > 0\text{)}, \tag{11}$$

the evolution of a, i.e. crack propagation, is governed by the Kuhn–Tucker conditions:

$$(G - G_c) \leq 0 \qquad \dot{a} \geq 0 \qquad (G - G_c)\dot{a} = 0. \tag{12}$$

2.2. Linear elastic interface

Let us consider the case in which the interface behaviour is modelled with the linear elastic CZM of Fig. 2(a), where the slope of the traction-separation law is denoted by k. The classical stress singularity at the crack tip of LEFM is obtained in the limit for $k \to \infty$. However, the equations in Section 2.1 are also valid for finite positive values of k. Note that in Fig. 2(a) no material failure is explicitly included in the material constitutive law.

A graphical representation of the power balance written in Eq. (2) is shown in Fig. 2(b) in terms of energy values and their increments when the crack propagates from the initial position a_0 to the new position $a_0 + \Delta a$. Point A in the figure corresponds to the displacement and force, v_A and F_A, at which the crack starts propagating. Since the response in the arms and on the interface is linear elastic up to this point, the potential energy Π_A stored in the body with initial crack a_0 is represented by the area OAA'O. Assume that, at point A the crack propagates by Δa, accompanied by an increase in the displacement from v_A to v_B and a decrease in the force from F_A to F_B. The total potential energy Π_B at point B is represented by the area OBB'O. The work done by the external force, ΔW, is equal to the area A'ABB'A'. Since $\Pi_A + \Delta W$ is the area OABB'O, the area OABO, shaded in grey in Fig. 2(b), is $\Pi_A - \Pi_B + \Delta W$, which represents the dissipated energy within the process, $\Delta\mathcal{D}$. Thus, the power balance (2) can be now written in terms of finite energy values as

$$\Pi_B - \Pi_A = \Delta W - \Delta\mathcal{D}. \tag{13}$$

The only part where this energy is dissipated is the interface where the crack propagates, i.e. at the crack tip. In this respect it is important to underline that, both in linear and nonlinear fracture mechanics, no material failure is included in the material constitutive law (see Fig. 2(a)). On the other hand, crack propagation effectively implies material failure at the crack tip, with associated dissipation. In the case of the linear elastic interface considered in this section, when the crack propagates the stress at the crack tip drops down to zero from a value σ_{max}. Therefore, as long as $\delta < \delta_c$, no energy is dissipated (Fig. 2(c)). When $\delta = \delta_c$, the work of separation, Ω, is instantaneously dissipated (Fig. 2(d)).

Therefore, in the finite propagation of the crack from a to $a + \Delta a$, the energy dissipated is equal to Ω times the new crack surface formed. From point A to point B, the new crack surface formed is $b\Delta a$ and it results:

$$\Delta\mathcal{D} = \Omega\, b\Delta a. \tag{14}$$

Dividing by $b\,\Delta a$, taking the limit for $\Delta a \to 0$, and comparing with (9) one then obtains

$$G_c = \frac{1}{b}\frac{\mathrm{d}\hat{\mathcal{D}}}{\mathrm{d}a} = \Omega. \tag{15}$$

Hence, when (before failure) the interface behaviour is linear elastic, the use of Griffith's LEFM crack propagation criterion, expressed in Eqs. (11) and (12), is equivalent to modelling the interface with the linear elastic CZM with brittle failure of Fig. 2(c and d).

2.3. Extension to the case of nonlinear potential-based constitutive law

Let us now consider the extension of the derivations in the previous section to what is normally called nonlinear fracture mechanics, or often 'elasto-plastic fracture mechanics' because initially the theory was developed for elasto-plastic problems (Anderson, 1995). It is well known that, within this theory, the elasto-plastic behaviour is approximated by path-independent laws, based on so-called 'deformation theory of plasticity' (Rice, 1968b). Likewise, if damage occurs instead of or in addition to plasticity, a path-independent law is used, too. Normally these laws can be considered as nonlinear elastic, but in this case we will consider laws which are indeed derived from a potential, as in elasticity, but also contain a softening part, in which material stability is lost. As material stability is typically considered a

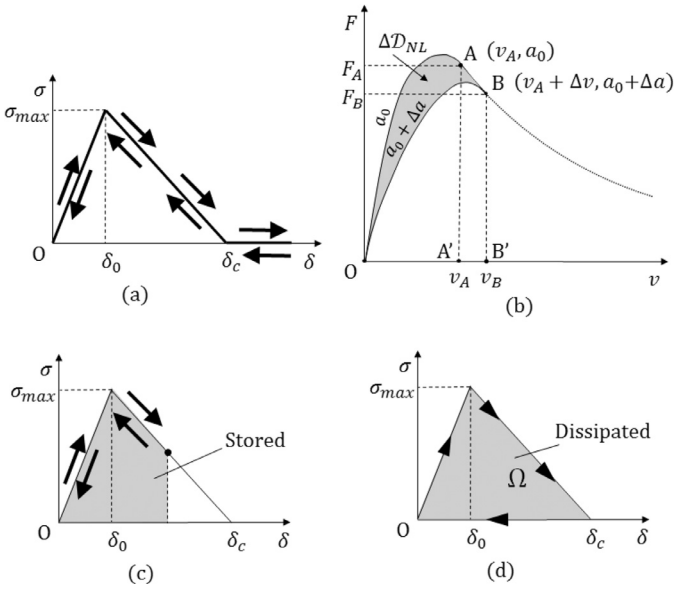

Fig. 3. Nonlinear potential-based interface behaviour: (a) potential-based traction-separation law (no material failure explicitly included) and (b) the associated structural response; equivalent CZM law for (c) an undamaged point and (d) a fully damaged one.

requirement for the behaviour to be called elastic, we will refer to this type of material behaviour as 'nonlinear potential-based'.

In particular, for the problems of interest in this article, let us consider the case in which the crack propagation process is modelled using the CZM of Fig. 3(a). In this model, once the maximum stress σ_{max} at the interface material is reached, softening starts occurring. However, (nonlinear) 'path-independent' response is assumed here so that, if the relative displacement at some point starts decreasing instead of continuously increasing, the curve followed during loading is followed back (as indicated by the arrows in Fig. 3(a)). Note also that in Fig. 3(a) no failure is explicitly included in the material law.

Again, the state of the system is univocally defined by the prescribed displacement and the crack length, so that the total potential energy can again be written as a function of v and a. Therefore, all the equations in Sections 2.1 and 2.2 still apply here, but we will now use subscript NL (referring to 'nonlinear') to the energy quantities, and therefore use symbols Π_{NL}, W_{NL}, $G_{c,NL}$ and $\mathcal{D}_{NL}$ to distinguish them from their counterparts in the LEFM case. Therefore, the energy balance written in rate form becomes

$$\dot{\Pi}_{NL} = \dot{W}_{NL} - \dot{\mathcal{D}}_{NL}, \tag{16}$$

and, following the arguments in Section 2.1, we still have

$$\dot{a} > 0 \qquad \Rightarrow \qquad -\frac{1}{b}\frac{\partial \Pi_{NL}}{\partial a} = G_{c,NL} = \frac{1}{b}\frac{\mathrm{d}\hat{\mathcal{D}}_{NL}}{\mathrm{d}a}. \tag{17}$$

Furthermore, Eq. (5) now becomes

$$\frac{\partial \Pi_{NL}}{\partial v} = F. \tag{18}$$

Also in this case, dissipation only occurs at the crack tip. Based on the same arguments made in Section 2.2, if the crack propagates when the relative displacement at the crack tip reaches the critical value δ_c in Fig. 3(a), then $G_{c,NL} = \Omega$, where $\Omega = \sigma_{max}\,\delta_c/2$. Vice versa, if $G_{c,NL} = \Omega$ in Eq. (17), then the crack propagates when $\delta = \delta_c$ at the interface.

Therefore, the use of crack propagation criterion (17) is equivalent to modelling the interface with the CZM of Fig. 3(c and d) and the the crack propagation criterion in quasi-static conditions becomes

$$\dot{a} > 0 \qquad \Rightarrow \qquad -\frac{1}{b}\frac{\partial \Pi_{NL}}{\partial a} = \Omega. \tag{19}$$

For this reason, in the future we will always use Ω instead of $G_{c,NL}$.

Once again, no failure is explicitly included in the material law in Fig. 3(a), according to which, in theory, even when $\delta > \delta_c$, upon reversal of δ the bilinear curve would be followed again. But this never happens because when $\delta = \delta_c$ crack propagation occurs. Therefore, in the equivalent CZM, if $\delta < \delta_c$ then the loading curve is followed upon reversal of δ (Fig. 3(c)), but if $\delta \geq \delta_c$, then upon reversal of δ the traction remains zero (Fig. 3(d)). In this respect, for simplicity, we will still refer to the CZM of Fig. 3(c-d) as potential based, with the understood meaning that the law is potential based only until $\delta < \delta_c$.

Remark 2.1. In the literature, the nonlinear energy release rate is often called J, and its critical value leading to crack propagation, J_c. This is because Rice (1968a) demonstrated that the J integral is equal to the nonlinear energy release rate:

$$J = \int_\Gamma \left(w\, n_x - \mathbf{t} \cdot \frac{\partial \mathbf{u}}{\partial x} \right) \mathrm{d}s = -\frac{1}{b}\frac{\partial \Pi_{NL}}{\partial a}, \tag{20}$$

where $\mathrm{d}s$ is a length increment along the chosen contour Γ, $\mathbf{t}$ and $\mathbf{u}$ are the tractions and displacements on Γ, n_x is the x component of the outward normal unit vector to Γ, x is the direction of crack propagation and w is the specific strain energy governing the constitutive law inside the chosen contour at all material points. According to this results, we should write

$$J_c = \Omega. \tag{21}$$

However, to the best of the authors' knowledge, it has never been emphasised that Rice's proof of Eq. (20) is based on the assumption that the material is homogeneous. This is because only when the material is homogeneous the following relationships used in Rice's proof holds true:

$$\frac{\partial w}{\partial x} = \frac{\partial w}{\partial \boldsymbol{\varepsilon}} \cdot \frac{\partial \boldsymbol{\varepsilon}}{\partial x} = \boldsymbol{\sigma}(\boldsymbol{\varepsilon}) \cdot \frac{\partial \boldsymbol{\varepsilon}}{\partial x} \tag{22}$$

where, $\boldsymbol{\sigma}$ and $\boldsymbol{\varepsilon}$ denote stress and strain tensors. When the material is non-homogeneous, w is a function of x not only through $\boldsymbol{\varepsilon}$, but also because of the variability of material properties along x. In other words, instead of writing $w = w(\boldsymbol{\varepsilon}(x))$ one should write $w = w(x, \boldsymbol{\varepsilon}(x))$, which invalidates (22), so that (20) is not valid either.

Obviously, in our case, the same argument can be made on the interface modelled with a CZM, in which the strain tensor $\boldsymbol{\varepsilon}$ should be replaced with the mode-I relative displacement, δ, and the stress tensor with the normal interface stress, σ. Therefore, for a non-homogeneous interface where the CZM parameters vary along x, generally one has

$$\frac{\partial w}{\partial x} \neq \sigma(\delta)\,\frac{\partial \delta}{\partial x}. \tag{23}$$

As a result, although the nonlinear critical energy release rate is always equal to Ω, it is only equal to J_c if the material within the chosen contour around the crack tip can be assumed homogeneous. We will see in the numerical results presented in Section 4.4 that, for the case of a non-flat R curve simulated via a CZM with variable material properties along x, $J_c \neq \Omega$.

Furthermore, because of (23), for a non-homogeneous interface one also has in general that

$$J \neq \int_0^{\delta_{CT}} \sigma(\delta_{CT})\,\mathrm{d}\delta_{CT}, \tag{24}$$

where δ_{CT} is the opening displacement at the crack tip. Therefore, in this case the CZM traction-separation law cannot be determined

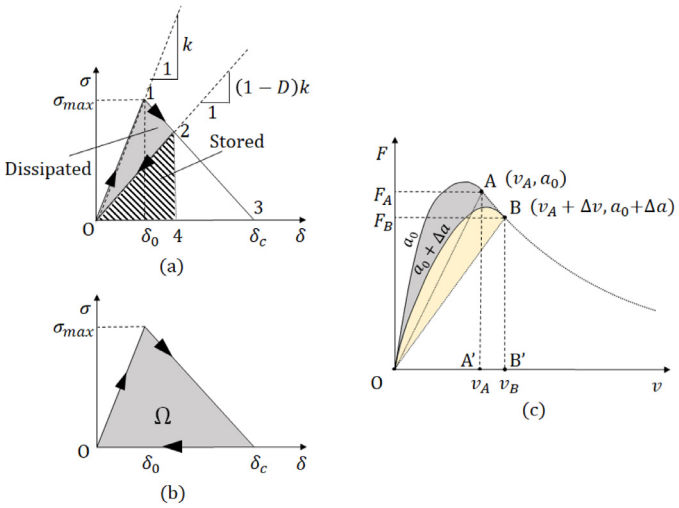

Fig. 4. Linear elastic CZM with progressive failure: traction separation law for (a) a partially damaged point and (b) a fully damaged point, and (c) the associated structural response. (For interpretation of the references to colour in this figure, the reader is referred to the web version of this article.)

as the derivative of the J integral with respect to the opening at the crack tip. This will also be shown in our numerical results in Section 4.4. □

Remark 2.2. As a second important remark, Rice's finding that "in infinitesimal (or rate with respect to geometrical size) form, the energy variation depends only on the strain energy of the material removed" (see page 209 of the seminal work by Rice, 1968a) is here obtained without his long mathematical derivation based on the J integral, which in Remark 2.1 we have actually shown to be valid only for homogeneous materials. When the CZMs of either Fig. 2(a) or Fig. 3(a) are used, the "strain energy removed" is indeed equal to the associated work of separation, Ω. In fact, with our derivation the fact that the nonlinear energy release rate is equal to Ω is an immediate result, valid indeed also for a non-homogeneous interface. □

All the other aspects of the discussion in the previous section remain almost unaltered from a conceptual point of view, including the balance of energy written in terms of finite increments through the graphical representation shown in Fig. 3(b), except that the shapes of the relevant areas representing work, stored and dissipated energies change, which is important for the derivation of the novel results in the next section. For example at point A, the potential energy $\Pi_{NL,\,A}$ is given by the area OAA'O, where now OA is a curve, and is equal to the external work done (note that a first part of the curve OA is a straight line until the stress at the initial crack tip reaches σ_{max}). If at point B, when the crack has propagated by an increment Δa, the prescribed displacement is reduced down to zero, the curve BO is followed (downward). If the prescribed displacement is increased again, the curve OB would be followed again (upward). Therefore, at point B, the potential energy $\Pi_{NL,\,B}$ is the area OBB'O, where again OB is a curve. If the increment of external work (area A'ABB'A') is then added to $\Pi_{NL,\,A}$ and $\Pi_{NL,\,B}$ is subtracted, the dissipation $\Delta\mathcal{D}_{NL}$, when the crack propagates from the initial length a_0 to the new one $a_0 + \Delta a$, is now the area shaded in grey and delimi ted by the two curved lines.

2.4. Extension to the case of linear elastic behaviour with progressive failure

Let us consider the same body studied previously, in which the interface is modelled with the CZM shown in Fig. 4(a) where the behaviour is linear elastic up to the relative separation δ_0 and the maximum traction σ_{max}, so that in this part $\sigma = k\delta$, with $k = \sigma_{max}/\delta_0$. For $\delta > \delta_0$, softening accompanied by damage dissipation and finally total debonding at the point where $\sigma = 0$ and $\delta = \delta_c$ occur. As long as $\delta < \delta_0$, all the work done to separate the interface remains stored as elastic energy. Once $\delta > \delta_0$, damage dissipation takes place, so that, if there were unloading, the secant straight-line to the origin would be followed, which shows that the energy represented by the triangle 0120, shaded in grey, has been dissipated. The remaining elastic energy is represented by the triangle 0240, which is hatched. When point 3 is reached, the total energy dissipated is equal to the area under the traction separation curve, Ω, as shown in Fig. 4(b).

The traction-separation law can be written in the classical damage-mechanics form:

$$\sigma = (1 - D)k\,\delta, \tag{25}$$

where the damage variable, D, is a function of the position x on the interface ($D = D(x)$). At each point, for a monotonically increasing δ, $D = 0$ for $\delta \le \delta_0$, $D = 1$ for $\delta \ge \delta_c$ and on the softening line ($\delta_0 < \delta < \delta_c$) D increases from 0 to 1.

For the monotonically increasing prescribed displacement considered here, points of the interface sufficiently close to the initial crack tip will experience a monotonically increasing relative displacement, δ. From a certain distance from the initial crack tip, interface points will first experience negative values of $\dot{\delta}$, leading to compressive interface stresses, until a maximum compressive stress is reached. After that, the relative displacements increase again, become positive and continue increasing monotonically. We make the widely adopted assumption that during the initial compressive phase no damage occurs so that, when the stress becomes tensile, the traction-separation law followed is the same as for the CZM of Fig. 3(c and d), because in both cases no displacement reversal occurs from the softening branch of the law. Therefore, the structural response under monotonically increasing prescribed displacement, v, (no reversal) is the same if either the CZM of Fig. 3(c and d) (nonlinear potential-based) or that of 4(a) are used.

Here it is extremely important to notice that new damage dissipation occurs only ahead of the crack tip on the part of the interface where $\delta \in (\delta_0,\ \delta_c)$, as already clarified from Fig. 4(a). Therefore, the body with an initial crack a_0 needs the external work represented by the area OAA'O (where OA is a curve) in the load–displacement plot of Fig. 4(c) to reach the force F_A and the displacement v_A, which is the point at which δ reaches δ_c at the initial crack tip, so that for further increase of the prescribed displacement the crack starts propagating. During this process, the material on the interface is initially acting as linear elastic, after which softening accompanied by damage occurs as the separation of some points at the interface becomes $\delta \in (\delta_0,\ \delta_c)$. If the direction of the prescribed displacement, v, were reversed from point A, the straight line AO would be followed in Fig. 4(c). This means that the triangle OAA'O represents the part of the external work stored as elastic energy, which in this case is the total potential energy Π_A, whereas the part OAO (where OA is a curve and AO a straight line) is energy dissipated due to damage at the interface ahead of the crack tip, and will be here denoted by $\Pi_{D,\,A}$.

The external work, area OAA'O, with OA a curve, would be equal to $\Pi_{NL,A}$ for the body with nonlinear potential-based behaviour considered in the previous section. It follows that

$$\Pi_{NL,A} = \Pi_A + \Pi_{D,A}. \tag{26}$$

As soon as at the crack tip $\delta = \delta_c$, the crack will start propagating if the prescribed displacement is further increased to values greater than v_A. In particular, when the prescribed displacement is $v_B > v_A$, the crack length will become $a_0 + \Delta a$, while the force de-

creases from F_A to F_B. The total external work done at that point is represented by the area OABB'O (where OAB is a curve).

If the body were unloaded from B, the straight line BO would be followed. This means that the potential energy stored at point B, Π_B, is the area of the triangle OBB'O. The unloaded body from point B would not be the same as one with an initial crack equal to $a_0 + \Delta a$, because the latter would have no damage developed ahead of the crack tip.

If the behaviour were nonlinear potential-based (Fig. 3), we have seen in Section 2.3 that the curve BO would be followed during unloading. In the present model with progressive failure, this would be equivalent to regaining the energy dissipated ahead of the crack tip (but not the energy previously dissipated behind the crack tip, on the newly formed crack surface of area $b\,\Delta a$). In other words, the area OBO (where OB is a curve and BO is a straight line), shaded in yellow in Fig. 4(c), represents the energy dissipated ahead of the crack tip at point B when the linear elastic CZM with progressive failure is used (Fig. 4(a and b)), and is therefore denoted by $\Pi_{D,B}$.

As already noted in Section 2.3, the area OBB'O (where OB is a curve) is equal to $\Pi_{NL,B}$. Ultimately, there follows

$$\Pi_{NL,B} = \Pi_B + \Pi_{D,B}, \tag{27}$$

or in general, at all times during crack propagation:

$$\Pi_{NL} = \Pi + \Pi_D, \tag{28}$$

where, as discussed above, Π_D is the energy dissipated ahead of the crack tip.

We noted that Π_{NL} is a function of v and a. Although this means that $\Pi + \Pi_D$ is a function of v and a, too, it is not obvious that the same applies to Π and Π_D separately. This is because the state of the interface with progressive damage is not defined by v and a only. Instead, in the most general case, it is defined by v and the damage variables $D(x)$ at each point x of the interface. On the other hand, we are considering cases in which the prescribed displacement is applied monotonically and we compute Π by considering the secant unloading straight line to the origin in the load–displacement curve, and calculating the area of the triangle between this line and the horizontal axis of the plot. This is equivalent to assuming that, for any v and for any $a > a_0$, Π is computed as follows: (i) a monotonically increasing displacement is prescribed until the crack length increases from a_0 to a; (ii) the damage is calculated at each point x of the interface and is denoted by $D_a(x)$; (iii) the prescribed displacement is then changed to reach the given value v, while the interface behaviour is assumed to be linear elastic with stiffness equal to $(1 - D_a(x))k$ at each point x of the interface. In this way, the damage profile is itself a function of a, and therefore Π is again a function of v and a.

As a result, Π_D is a function of v and a at most, too. However, Π_D only depends on a. This is because, for fixed a, Π is computed assuming linear elastic behaviour (with reduced stiffness at some points for $a > a_0$) and, therefore, $\partial\Pi/\partial v = F$. Comparing with Eq. (18), we have

$$\frac{\partial \Pi}{\partial v} = \frac{\partial \Pi_{NL}}{\partial v} = F. \tag{29}$$

From Eq. (28) we then get

$$\frac{\partial \Pi_D}{\partial v} = \frac{\partial \Pi_{NL}}{\partial v} - \frac{\partial \Pi}{\partial v} = 0, \tag{30}$$

which means that Π_D is only a function of a. Ultimately, replacing Eq. (28) in Eq. (19), and because Π_D only depends on a, we have

$$\dot{a} > 0 \quad \Rightarrow \quad \Omega = -\frac{1}{b}\frac{\partial \Pi}{\partial a} - \frac{1}{b}\frac{\mathrm{d}\Pi_D}{\mathrm{d}a}. \tag{31}$$

If, during crack propagation, we can compute $\partial\Pi/\partial a$ and we continue defining G_c as the total potential energy released per unit new crack area formed during crack propagation:

$$\dot{a} > 0 \quad \Rightarrow \quad -\frac{1}{b}\frac{\partial \Pi}{\partial a} = G_c, \tag{32}$$

we then find:

$$\dot{a} > 0 \quad \Rightarrow \quad \Omega = G_c - \frac{1}{b}\frac{\mathrm{d}\Pi_D}{\mathrm{d}a}. \tag{33}$$

For the case of an homogeneous material $J_c = \Omega$ and the following relationship is found between the critical J integral value and the critical energy release rate G_c:

$$J_c = G_c - \frac{1}{b}\frac{\mathrm{d}\Pi_D}{\mathrm{d}a}. \tag{34}$$

The above results show that the difference between G_c and Ω, and between G_c and J_c for a homogeneous interface, is not to be attributed to the size of the cohesive zone, but to the variation of the amount of energy already dissipated ahead of the crack tip during crack propagation. In other words, if the profile of the specific energy dissipated ahead of the crack tip remains unaltered during crack propagation, and therefore translates in a steady-state fashion together with the crack tip, then $\Omega = G_c$.

In the following sections we will show that such a steady-state process is actually found for a DCB with prescribed rotations, modelled with a CZM with linear elastic damage and progressive failure, so that an exact data-reduction scheme based on LEFM provides a value of G_c equal to Ω. For the case of a homogeneous interface, we will therefore find that $G_c = J_c$, so that the use of LEFM or the J integral provides exactly the same result.

An even more important result is that, for the much more widely used case of a DCB loaded with a prescribed cross-head displacement, although the profile of the specific dissipation ahead of the crack tip does not advance in steady-state, $\mathrm{d}\Pi_D/\mathrm{d}a$ is normally small with respect to Ω, even when the size of the cohesive-zone is extremely large. In fact, we will show in Sections 4 and 5 that, for the case of a flat R-curve, $\mathrm{d}\Pi_D/\mathrm{d}a$ is indeed extremely small and negligible in most engineering applications. For the case of a significantly rising R-curve, results in Section 4.4 will show that the discrepancy between G_c and Ω can be still quite limited.

Data-reduction schemes based on LEFM effectively assume that the fracture resistance is given by G_c. Therefore, the practical implication of the theoretical result summarised in Eq. (33) is very important, because this equation shows that G_c can indeed be very close to Ω. In turn, this means that LEFM-based methods can be extremely effective, as long as G_c itself can be computed with sufficient accuracy.

In Section 3 we will present a rigorous analysis which shows that G_c can indeed be estimated with very good accuracy for typical DCB specimens without the need for measuring the crack length during an experiment, and also that such accuracy can be a priori estimated. In this way, in Sections 2 and 3 we provide a sound theoretical foundation for a data-reduction scheme for a DCB loaded with forces which is very accurate and much simpler, and therefore much more practical and convenient, than those in the current standards.

Remark 2.3. Although we have considered CZMs with a bi-linear traction-separation law, it is worth noting that all our results obtained in Section 2 are valid also when a different shape of the traction-separation law is used, as long as the unloading response of the CZM is linear.

3. Determination of G_c and J_c for a DCB specimen

Let us consider a DCB specimen tested in mode I where either displacement or rotation is prescribed at the loaded ends of the arms, as shown in Fig. 5(a) and (b), respectively. We are assuming

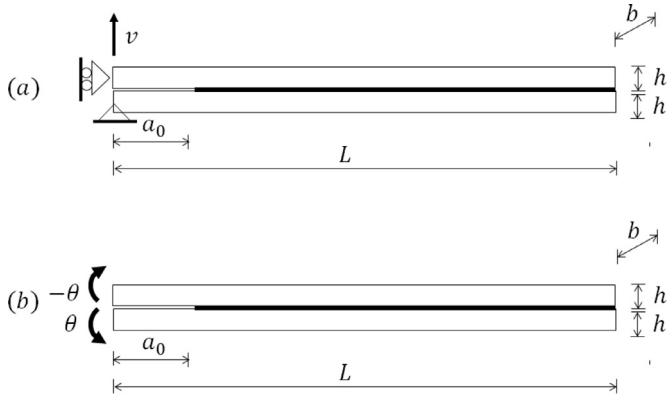

Fig. 5. 2D DCB model, showing prescribed (a) cross-head displacement v and (b) rotations θ.

that the loading speed is sufficiently low to make inertia effects and temperature variations negligible. The length, width and depth of each arm are denoted by L, b and h, respectively, with $h \ll L$.

The cross-head displacement opening v is prescribed and monotonically increasing upwards, as shown in Fig. 5(a). Furthermore, rotations, θ, of the end sections are prescribed equal and opposite, each one again monotonically increasing in absolute value, and θ is positive if counter-clockwise (see Fig. 5(b)). An initial crack is present with length a_0, measured from the line of application of the forces. It is convenient to consider the general case in which both v and θ can be prescribed at the same time, as a function of time t, although in practical experimental tests only one of them is prescribed. In fact, the case in which v is prescribed is by far the most frequent and the only one considered in industrial standards. The self-weight of the DCB is not considered not only for simplicity, but also because its contribution is effectively negligible in most cases of practical interest.

Rate-dependent effects may be important in some applications. However, we will not take them into account because it is typical in practical engineering applications to ignore them when the fracture resistance is determined for a certain applied loading rate, and then to evaluate their importance, if any, by performing tests at different loading speed.

Assuming constant width, b, symmetry justifies the use of a 2D solid continuum model, but, because $h \ll L$, beam theories are sufficiently effective and widely used. Therefore, we will assume the DCB is a 2D body undergoing an isothermal, quasi-static, rate-independent deformation process. We will also assume that strains, displacements and rotations are sufficiently small so that a geometrically linear model is sufficiently effective. It was shown in Škec and Jelenić (2017) that this is a valid assumption because differences between using a geometrically linear or nonlinear formulation become noticeable only when displacements and rotations of the specimen are relatively large compared to the specimen dimensions.

As we already mentioned, in experimental testing either v only or θ only is typically prescribed. For each separate case, because the behaviour is linear elastic with damage, using geometrically linear beam theories, the total potential energy is given by

$$\Pi_v(v,a) = \frac{F\,v}{2} \quad \text{or} \quad \Pi_\theta(\theta,a) = M\,\theta, \tag{35}$$

where $F = F(v,a)$ and $M = M(\theta,a)$ are the reaction force and moment.

Thus, for these two types of experiments, expressions from Eq. (35) provide the total potential energy for any value of a, whose partial derivative with respect to a would provide G_c. These values of G_c will be equal to Ω only when the second term on the right-hand side of Eq. (33) is zero, which is the case if the propagation of the specific-dissipation profile ahead of the crack tip is steady-state.

In this section we analyse two cases: DCB with prescribed displacements (non-steady-state crack propagation) and DCB with prescribed rotations (steady-state crack propagation).

3.1. DCB with prescribed displacement

Let us first consider the case where the displacement is prescribed, so that we use formula $(35)_1$ for Π_v. In order to take the derivative with respect to a, Π_v has to be expressed in terms of a. As mentioned in the introduction, F, v and a can be related using formulae from simple beam theories, but we have to be aware that the crack length in these formulae is not the actual crack length a, but an equivalent crack length, which will either be denoted by a_{eq}, to refer to the general case, or by a_{eqE} or a_{eqT} to specify that the Euler–Bernoulli or Timoshenko beam theory is considered, respectively.

The difference between the actual and the equivalent crack length is due to the fact that, regardless of the beam theory used, the deflection formulae are based on the assumption that the arms of the DCB are perfectly clamped at the crack tip. Instead, the cross sections at the crack tip are normally characterised by both a displacement and a rotation as a result of the deformation of the interface and of the beam in front of the crack tip. Therefore, the equivalent crack length is defined as the length that the crack should have to make the formulae correct if the arms were really clamped at the crack tip, for given values of F and v.

Thus, for Euler–Bernoulli beam theory a_{eqE} is defined by

$$v = 2\frac{F\,a_{eqE}^3}{3\,EI} \quad \Rightarrow \quad a_{eqE} = \sqrt[3]{\frac{3\,v\,EI}{2\,F}}, \tag{36}$$

where E is the effective Young's modulus and $I = bh^3/12$ is the second moment of area of each DCB arm. For Timoshenko beam theory a_{eqT} is defined by

$$v = 2\left(\frac{F\,a_{eqT}^3}{3\,EI} + \frac{F\,a_{eqT}}{\mu A_s}\right) \quad \Rightarrow \quad a_{eqT} = \frac{\sqrt[3]{B^2} - \sqrt[3]{12}C_1}{\sqrt[3]{18\,B}}, \tag{37}$$

where μ is the shear modulus, $A_s = A\,k_s$ ($A = bh$ is the area of the cross-section of DCB arms and k_s is the shear correction coefficient) and

$$B = \sqrt{12\,C_1^3 + 81\,C_2^2} + 9\,C_2, \quad C_1 = \frac{3\,EI}{\mu A_s}, \quad C_2 = \frac{3\,EI\,v}{2\,F} = a_{eqE}^3. \tag{38}$$

Letting $\mu A_s \to \infty$ leads to $C_1 = 0$, $B = 18\,C_2$ and $a_{eqT} = \sqrt[3]{C_2} = a_{eqE}$, which is the expected result.

Because of the crack tip displacement and rotation, the total potential energy Π_v cannot be expressed in terms of the actual crack length, but only in terms of the equivalent crack lengths depending on the beam theory used, i.e.

$$\Pi_v(v,a) = \Pi_v^E(v, a_{eqE}(a)), \quad \text{or} \quad \Pi_v(v,a) = \Pi_v^T(v, a_{eqT}(a)). \tag{39}$$

It follows that during crack propagation (i.e. $\dot{a} > 0$, see Eq. (32)):

$$G_c = -\frac{1}{b}\frac{\partial \Pi_v}{\partial a} = -\frac{1}{b}\frac{\partial \Pi_v^E}{\partial a_{eqE}}\frac{\mathrm{d}a_{eqE}}{\mathrm{d}a} = -\frac{1}{b}\frac{\partial \Pi_v^T}{\partial a_{eqT}}\frac{\mathrm{d}a_{eqT}}{\mathrm{d}a}. \tag{40}$$

Note that, although we will not emphasise it each time for the sake of simplicity, all the following expressions for G_c are derived under the assumption that $\dot{a} > 0$. Thus, these expressions are valid

only if the values of v and F are obtained (measured) during crack propagation. Substituting F in (35) using (36) gives

$$\Pi_v^E = \frac{3\,EI\,v^2}{4\,a_{eqE}^3}, \tag{41}$$

which substituted in Eq. (40) results in

$$G_c = \frac{9\,EI\,v^2}{4\,b\,a_{eqE}^4}\frac{\mathrm{d}a_{eqE}}{\mathrm{d}a} = G_c^E\frac{\mathrm{d}a_{eqE}}{\mathrm{d}a}, \tag{42}$$

where G_c^E denotes the value of G_c which would be obtained for $\mathrm{d}a_{eqE}/\mathrm{d}a = 1$.

In a similar fashion, for Timoshenko beam theory, substituting F in (35) using (37) gives

$$\Pi_v^T = \frac{v^2}{4}\frac{3\,EI\,\mu A_s}{\mu A_s\,a_{eqT}^3 + 3\,EI\,a_{eqT}}, \tag{43}$$

and then

$$G_c = \frac{v^2}{4b}\frac{9\,EI\,\mu A_s(EI+\mu A_s\,a_{eqT}^2)}{(\mu A_s\,a_{eqT}^3 + 3\,EI\,a_{eqT})^2}\frac{\mathrm{d}a_{eqT}}{\mathrm{d}a} = G_c^T\frac{\mathrm{d}a_{eqT}}{\mathrm{d}a}, \tag{44}$$

where G_c^T denotes the value of G_c which would be obtained for $\mathrm{d}a_{eqT}/\mathrm{d}a = 1$.

Using Eqs. (36) and (37), G_c^E and G_c^T can also be expressed in terms of F and a_{eqE} or a_{eqT} as

$$G_c^E = \frac{F^2 a_{eqE}^2}{bEI} \quad \text{and} \quad G_c^T = \frac{F^2}{b}\left(\frac{a_{eqT}^2}{EI} + \frac{1}{\mu A_s}\right). \tag{45}$$

Similar expressions for G_c can be found in the literature and standards, but in those expressions a is used instead of a_{eq}.

Remark 3.1. Overlooking the difference between a and a_{eq} can lead to substantial errors in computing G_c (note that a_{eq} in Eq. (45) is squared). Furthermore, in the general case $\mathrm{d}a_{eqE}/\mathrm{d}a \neq 1$ and $\mathrm{d}a_{eqT}/\mathrm{d}a \neq 1$, and thus $G_c^E \neq G_c$ and $G_c^T \neq G_c$. In Section 4, for a typical problem we will show how big exactly the error in computing G_c is when in formula (45) a is used instead of a_{eqE} or a_{eqT}. □

In formulae (45), a_{eqE} and a_{eqT} can be expressed in terms of F and v from Eqs. (36) and (37), respectively. For example, replacing $(36)_2$ into $(45)_1$ gives

$$G_c^E = \sqrt[3]{\frac{9F^4v^2}{4b^3EI}}. \tag{46}$$

The expression for G_c^T is more convoluted if given explicitly in terms of F and v. It follows from

$$G_c^T = \frac{F^2}{b}\left(\frac{a_{eqT}^2(v,F)}{EI} + \frac{1}{\mu A_s}\right), \tag{47}$$

where $a_{eqT}(v, F)$ is given by $(37)_2$ and (38).

An expression for G_c analogous to Eq. (46) has been already reported in the literature (Biel and Stigh, 2007; Alfano et al., 2011), but in that approach, although it is not stated, it is effectively, and incorrectly, assumed that $a = a_{eqE}$. This is because the derivative of Π_v is taken with respect to a_{eq} instead of a. The same argument applies to expression (47) for G_c^T although, to the best of authors' knowledge, only numerical methods for determining a_{eqT} were suggested (Lopes et al., 2016), and the derivative $\mathrm{d}a_{eqT}/\mathrm{d}a$ was again not taken into account.

The main advantage of formulae (46) and (47) is that they do not require the measurement of the actual crack length a, which excludes one main source of errors in the determination of G_c. Instead, v and F can be measured quite accurately and easily using standard tensile-testing machines.

On the other hand, formulae (46) and (47) provide an approximation of the exact value of G_c, which is only obtained if the value of G_c^E or G_c^T are multiplied by the derivatives of a_{eqE} or a_{eqT} with respect to a, as shown in Eqs. (42) and (44). Therefore, in Sections 4 and 5, in order to better analyse the accuracy of formulae (46) and (47) for G_c^E and G_c^T, we also compute the values of these derivatives for different problems. To compute such derivatives, we obviously need the value of a, which would have to be measured in a real experiment. This is one of the reasons why in Sections 4 and 5 'virtual experiments', rather than real ones, are performed.

We will also show that, independently from the beam theory used, the same value G_c is obtained when the corresponding derivative is taken into account, which is in accordance with Eq. (40).

3.2. DCB with prescribed rotations

Now we examine the case where, instead of a displacement, equal and opposite rotations θ are applied on the end sections of the DCB arms as shown in Fig. 5(b) (Sørensen and Jacobsen, 2003; Rice, 1968b; Freiman et al., 1973; Sørensen et al., 1996; Lindhagen and Berglund, 2000; Sørensen, 2002). In order to prescribe a desired rotation, it is necessary to apply a concentrated moment M at the same point. This means that the DCB arms will be in pure bending and if we assume that they act like cantilever beams we can use the simple beam formula:

$$\theta = \frac{M\,a_{eq}}{EI}, \tag{48}$$

where a_{eq} is the same for Euler–Bernoulli and Timoshenko beam theories since in pure bending there are no shear strains. Using this formula and expression $(35)_2$ for Π_θ we obtain

$$\Pi_\theta(\theta, a) = \overline{\Pi}_\theta(\theta, a_{eq}(a)) = \frac{\theta^2\,EI}{a_{eq}}, \tag{49}$$

and then write

$$G_c = -\frac{1}{b}\frac{\partial\Pi_\theta}{\partial a} = -\frac{1}{b}\frac{\partial\overline{\Pi}_\theta}{\partial a_{eq}}\frac{\mathrm{d}a_{eq}}{\mathrm{d}a} = \frac{\theta^2\,EI}{b\,a_{eq}^2}\frac{\mathrm{d}a_{eq}}{\mathrm{d}a}. \tag{50}$$

Substituting θ from Eq. (48) gives

$$G_c = \frac{M^2}{bEI}\frac{\mathrm{d}a_{eq}}{\mathrm{d}a}. \tag{51}$$

Note that, in accordance with Eq. (32), in Eq. (50) it is assumed that $\dot{a} > 0$, which means that Eq. (51) is valid only if the value of M is obtained (measured) during crack propagation. However, only the moment at the crack tip (which is equal to M, whereas the value of the shear force is zero) is responsible for opening the crack and making it propagate. This means that for any crack tip position a the crack will propagate when a certain critical value of M is reached. Thus, as long as the crack tip is sufficiently far away from the end of the DCB specimen, constant boundary conditions at the crack tip for any position of the crack will result in a steady-state crack propagation, where $a_{eq} = a + c$, with c a constant. In turn, this results in $\mathrm{d}a_{eq}/\mathrm{d}a = 1$. From Eq. (51) it then follows that

$$G_c = \frac{M^2}{bEI}, \tag{52}$$

for any position of the crack tip.

Furthermore, the steady-state nature of the crack propagation, which will be confirmed by the numerical results reported in Section 4, also means that the profile of the specific dissipation in front of the crack tip translates together with the crack tip. This means that $\mathrm{d}\Pi_D/\mathrm{d}a = 0$ in Eq. (33) so that $G_c = \Omega$ exactly. Therefore, formula (52) can be successfully used to determine the cohesive law of the adhesive. However, in terms of standard procedures

for determining G_c, performing experiments by prescribing the displacement is still considerably simpler and, as we will show in the following sections, it can give efficient and accurate estimation of G_c without the need for the measurement of the crack length.

3.3. Characterisation of fracture resistance based on the J integral

As discussed in Section 2.3, based on Eq. (21), it has been argued by many authors that the critical value of the J integral, J_c, provides the most accurate prediction of Ω, although we explained in the same section why this is actually true only if the material is homogeneous.

Based on Euler–Bernoulli beam theory, for a DCB with prescribed displacements, J_c is given by the formula equivalent to the one provided by Paris and Paris (1988) and Olsson and Stigh (1989), and will be denoted by J_c^E:

$$J_c^E = -\frac{2F\theta_v}{b}, \tag{53}$$

where θ_v is the rotation of the cross section at the point of the application of the force F, whereas F and v are those measured during crack propagation. Also, note that the minus sign is the result of the sign convention used for the rotations in Fig. 5(b).

An analogous formula, again for the case of prescribed displacements but based on Timoshenko beam theory, is not available in the literature, to the best of the authors' knowledge, but it can be derived as shown in Appendix A. Denoting this value as J_c^T we obtain

$$J_c^T = \frac{F^2}{b}\left(\frac{1}{\mu A_s} - \frac{2\theta_v}{F}\right). \tag{54}$$

In case of prescribed rotations, the expression of J_c (Rice, 1968b) is the same for both beam theories and equal to the expression of G_c in Eq. (52).

When the traction separation law is constant along the interface, the same formulae as (53) and (54) can be derived by directly calculating Ω via the solution of the differential equations of the DCB undergoing crack propagation. For Euler–Bernoulli theory, this was proved by Olsson and Stigh (1989). For Timoshenko theory and a DCB with both prescribed displacement and rotations, the derivation is provided in Appendix B.

It is worth underlining that both formulae (53) and (54) require the measurement of the end rotations of specimens. This makes them impractical, which is also why this paper focuses more on the computation of G_c rather than J_c.

4. Accuracy of LEFM-based formulae, influence of interface ductility and comparison with standards

In this section, using the data from virtual experiments, we will show how accurate Formulae (46), (47) and (52) for G_c^E, G_c^T and G_c, respectively, are in predicting the area Ω under the traction-separation curve of the CZM used. Additionally, we will numerically compute the values of the derivatives da_{eq}/da for Euler–Bernoulli and Timoshenko beam theories, also to verify that the same value of G_c is obtained for both beam theories once these derivatives are taken into account using Eqs. (42) and (44), in accordance with Eq. (40).

4.1. Virtual experiments considered and details of the FE simulations

The input data, which includes v, θ and a, as well as F for a DCB with prescribed displacement (Fig. 5(a)) and M for the one with prescribed rotations (Fig. 5(b)), is not actually measured from real experiments, but created by conducting accurate FE simulations. Because the DCB test is symmetric with respect to the interface mid-plane, only the upper half of the specimen is modelled.

Table 1
Geometric data used in the virtual experiments in Section 4.

L [mm]	h [mm]	b [mm]	a_0 [mm]
200	6	25	30

Table 2
Material data used in the virtual experiments in Section 4.

E [GPa]	ν [-]	k_s [-]	Ω [N/mm]	σ_{max} [MPa]	δ_c [mm]	δ_0 [mm]
70	1/3	5/6	1	{7.5, 15, 30, 60, 120}	$2\,\Omega/\sigma_{max}$	$0.01\,\delta_c$

The bi-linear CZM with progressive failure shown in Fig. 4(a and b), in which unloading occurs according to the secant line to the origin, is used as the constitutive model for the interface elements used on the DCB interface. The material and geometric data used in the virtual experiment is presented in Tables 1 and 2 and correspond to a typical adhesive joint between two aluminium components. Since the objective here is to assess how the ductility of the adhesive influences the range of validity of LEFM for problems with large cohesive zones ahead of the crack tip, different simulations have been conducted varying σ_{max} with the set of values shown in Table 2. Further analyses with other types of materials (i.e. steel and CFRP), dimensions and adhesives will be presented in Section 5.

A total number of 2000 2-node Timoshenko beam elements are distributed evenly over the upper half of the DCB, meaning that the element length is 0.1 mm. Such a fine mesh is used to eliminate, or at least minimise, the influence of discretisation-caused spurious oscillations on the results (Alfano and Crisfield, 2001; Škec et al., 2015). A 4-node interface element is attached to every beam FE from $x = a_0$ to $x = L$ making a total of 1700 interface elements. Beam FEs are integrated using the one-point Gauss quadrature, while the interface elements are integrated using the 3-point Simpson's rule.

Displacement control is used with a total prescribed displacement of 10 mm, subdivided into 100 equal increments. Newton–Raphson solution procedure was used with a tight numerical tolerance to assess convergence.

Remark 4.1. The analysis can be easily performed using geometrically nonlinear beam finite elements based on Reissner's beam theory (Škec and Jelenić, 2017), which is needed in cases when displacements and rotations of DCB arms are not small. However, the observed influence of geometrical nonlinearity for the range of displacements and rotations in the present analyses was found to be negligible and the use of Timoshenko beam FEs is therefore justified.

Remark 4.2. It is very important to note that the use of 2D geometrically linear Timoshenko finite elements is the most appropriate choice for a proper comparison of the data-reduction methods investigated in this work. This is because all these methods are based either on Euler–Bernoulli or Timoshenko beam theories, and always in the geometrically linear case. Therefore, any more sophisticated model for the virtual experiments, e.g. higher order beam theories and/or 2D or even 3D models, would introduce some discrepancies for all the methods studied. Such discrepancies would actually be extremely small because 2D beam theories have been proved to be very effective, which is the reason why they are used in standards. On the other hand, these small discrepancies would still make the comparison less clear. For example, for a flat R-curve J_c^T would not exactly be equal to Ω. Moreover, analytical solution for Euler–Bernoulli DCB with progressive damage (Dimitri et al., 2017) could be used for virtual experiments, but in

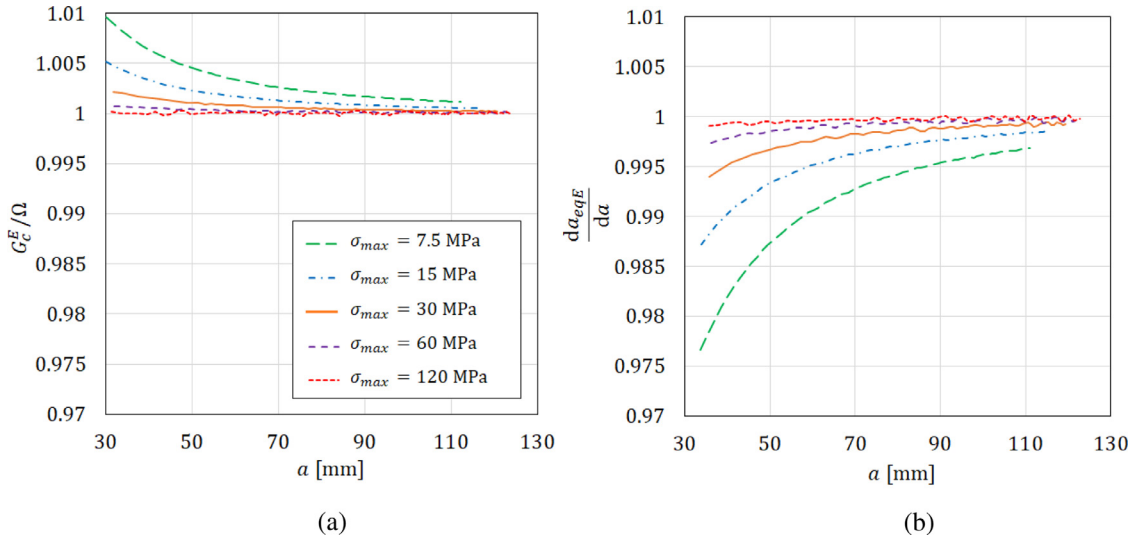

Fig. 6. Values of (a) G_c^E/Ω and (b) da_{eqE}/da for different values of σ_{max}

that case the influence of shear deformability of the arms could not be appreciated in the analysis.

4.2. DCB with prescribed displacement

Figs. 6–9 report the results obtained when the DCB is loaded with a prescribed displacement, v.

In Fig. 6, G_c^E and the corresponding derivative da_{eqE}/da are shown against the crack length, a, where G_c^E is recovered from the numerical results for F and v using (46), while da_{eqE}/da is computed numerically from (36) upon detecting the actual crack length a for every considered pair (F, v). Oscillations which appear in Fig. 6 for $\sigma_{max} = 120$ MPa are a numerical artefact caused by the discretisation in the numerical model and can be eliminated by using an even finer FE mesh (Alfano and Crisfield, 2001; Škec et al., 2015). The case with oscillations, unlike all the others, also showed some minor convergence problems of the nonlinear solution procedure (the displacement increment needed to be reduced by 50% on two occasions).

If by a_i we denote the actual crack length obtained from a virtual measurement i ($i = 1, 2, \ldots, n$, where n is the total number of virtual measurements during crack propagation), we can compute $a_{eq,i}$ from v_i and F_i. The derivative da_{eqE}/da, corresponding to the virtual measurement i, is computed using a 5-point central difference formula accounting for variable distance between points (Holoborodko, 2017), whose general expression is

$$\left.\frac{da_{eq}}{da}\right|_{a=a_i} \approx \sum_{j=1}^{(N-1)/2} c_j \frac{a_{eq,i+j} - a_{eq,i-j}}{a_{i+j} - a_{i-j}} 2j, \tag{55}$$

where N is the number of points used. In our case, $N = 5$, $j = 1, 2$, $c_1 = 1/4$ and $c_2 = 1/8$ (Holoborodko, 2017). From this formula it is clear why the derivative could not be calculated for the first two and the last two recorded values of the crack propagation.

Fig. 6 shows that the higher σ_{max} and the longer the crack has propagated, the better G_c^E approximates Ω and the closer to unity da_{eqE}/da is. We clearly see that $da_{eqE}/da < 1$ for short cracks and low σ_{max} values, but it converges to 1 for with larger cracks and higher values of σ_{max}. Furthermore, after few millimetres of crack propagation from the initial position, the influence of the derivative is less than 2% even for the minimum considered value of σ_{max}, equal to 7.5 MPa. For larger values of σ_{max}, the influence quickly falls below 1%.

Unlike Euler–Bernoulli beam theory, from Fig. 7 we can see that G_c^T and da_{eqT}/da, computed from (47) and numerically from (37), do not converge to Ω as $\sigma_{max} \to \infty$. The explanation for this lies in the fact that, when Timoshenko beam theory is used (which it is in our numerical model), due to shear deformability, even an infinitely rigid and brittle interface cannot prevent rotations at the crack tip to occur. Thus, assuming that the arms of a Timoshenko DCB are clamped at the crack tip (which is done in the derivation of the formula for G_c^T) is not equivalent to letting $\sigma_{max} \to \infty$ at the interface in our numerical model. In Appendix C we explain the results shown in Fig. 7 and derive exact formulae for the limit values of G_c^T/Ω and da_{eqT}/da obtained when $\sigma_{max} \to \infty$ and denoted by $\sigma_{max} = \infty$ in Fig. 7.

In accordance with Eqs. (42) and (44), the same value of G_c must be obtained independently of the beam theory used, i.e. it must be

$$G_c^E \frac{da_{eqE}}{da} = G_c^T \frac{da_{eqT}}{da} = G_c \tag{56}$$

Values of G_c obtained using different beam theories are presented for different values of σ_{max} in Fig. 8(a). For $\sigma_{max} = 7.5$ MPa, the dashed green line is obtained by multiplying G_c^E by da_{eqE}/da, while the green circular markers are obtained by multiplying G_c^T by da_{eqT}/da. The results clearly overlap and the same happens for all other values of σ_{max}, although it is not reported for the sake of clarity. Furthermore, from Fig. 8(a) it can be clearly seen that G_c is approaching Ω as the value of σ_{max} increases. In accordance with Eq. (33), the difference between G_c and Ω is to be attributed to the fact that, for a DCB with prescribed displacement, the crack propagation process is not steady-state, as shown later below in Fig. 9 and therefore $d\Pi_D/da \neq 0$. On the other hand, the fact that such difference is mostly less or far less than 1% is because the process is actually very close to steady-state. Furthermore, the longer the crack propagation, the closer to being steady-state the process is.

Interestingly enough, we can notice that formulae for G_c^E and G_c^T give a better approximation of Ω than the exact formula for G_c, which includes the derivative da_{eq}/da. This is because, for both beam theories, not taking into account the derivative da_{eq}/da in expressions for G_c^E and G_c^T somehow partially compensates the discrepancy between G_c and Ω due to the process not being steady-state. In any case, these results, which cover a wide range of adhesive behaviour (from extremely brittle to extremely ductile), suggest that formulae (46) and (47) for G_c^E and G_c^T, which do not require the mesurement of the crack length, can be used as very

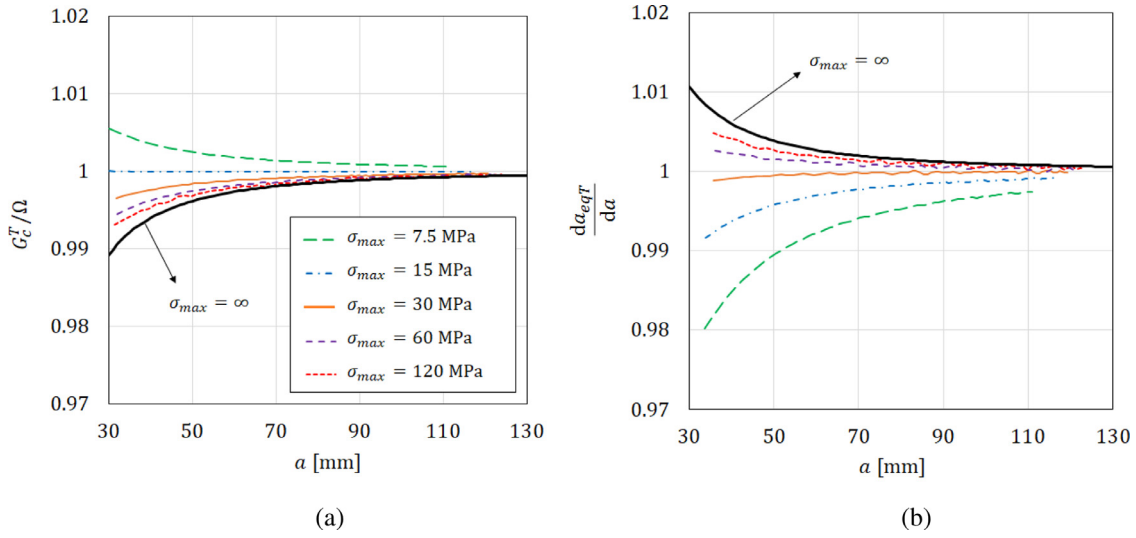

Fig. 7. Values of (a) G_c^T/Ω and (b) da_{eqT}/da for different values of σ_{max}

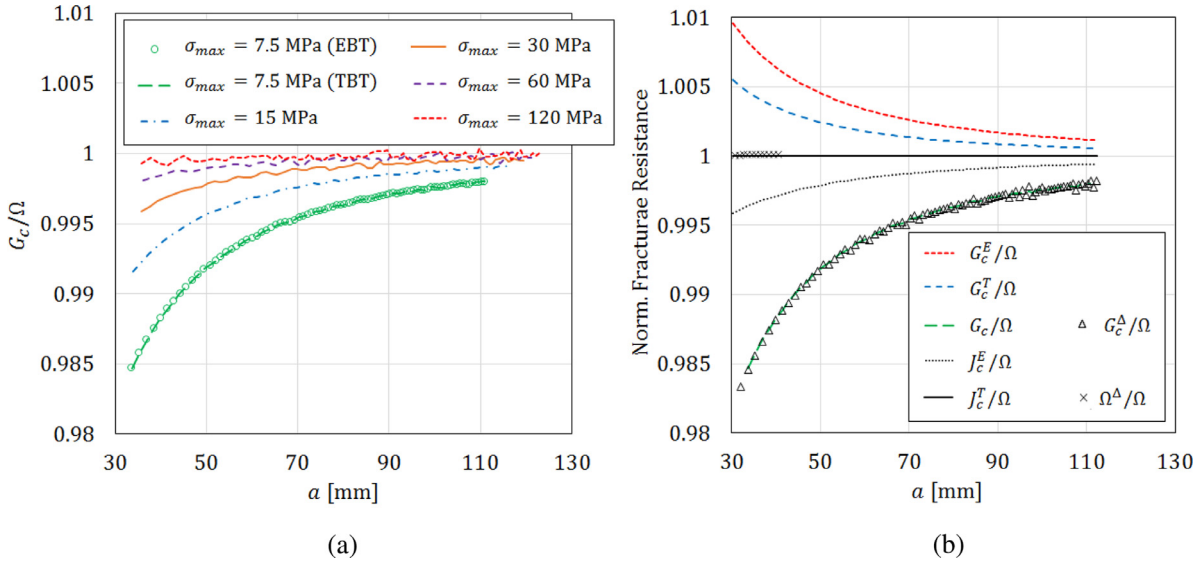

Fig. 8. Values of: (a) G_c/Ω for different values of σ_{max} and (b) different fracture resistance parameters normalised with respect to Ω obtained for $\sigma_{max} = 7.5$ MPa. (For interpretation of the references to colour in this figure, the reader is referred to the web version of this article.)

simple, accurate and practical data reduction schemes. This finding is further confirmed by the numerical results presented in Section 5, where predictions given by these formulae are compared to those provided by the data-reduction schemes used in BS ISO 25217:2009 (2009) for DCB specimens with different material and geometric properties taken from real experimental data reported in the literature.

In Fig. 8(b) we have compared the values of G_c^E, G_c^T and G_c for the most ductile case ($\sigma_{max} = 7.5$ MPa) with the values for J_c according to Eqs. (53) and (54), as well as with the definitions for G_c and Ω as given in Eqs. (8) and (19). For the latter, partial derivatives have been approximated by finite differences, i.e.

$$G_c \approx G_c^\Delta = -\frac{1}{b}\frac{\Delta\Pi}{\Delta a} \quad \text{and} \quad \Omega \approx \Omega^\Delta = -\frac{1}{b}\frac{\Delta\Pi_{NL}}{\Delta a}, \tag{57}$$

where Π and Π_{NL} are calculated according to Fig. 4 and the discussion in Section 2.4 using the $F-v$ data obtained from our numerical model. Notice that, to compute Ω for any crack length a using Eq. $(57)_2$, an undamaged specimen with initial crack length $a+\Delta a$ is required. Therefore, the calculation is restarted with the increased initial crack length each time the crack has propagated by an amount Δa. In Fig. 8(b) only the first ten values for Ω^Δ are shown, which is enough to show that the approximation for Ω^Δ in Eq. $(57)_2$ is indeed very accurate. However, determining G_c and Ω using Eq. (57) requires the measurement of crack length, which makes them less practical in real-life applications.

As expected, results obtained using Eq. (57) perfectly match the values of G_c and J_c^T obtained using formulae (56) and (54). As already mentioned, formulae for G_c^E and G_c^T provide values very close to Ω. When shear strains are neglected in Eq. (54), formula (53) for J_c^E fails to give the exact area under the traction-separation law of the CZM used. In this example, even for the extremely ductile case, the accuracy of the formula for G_c^T is comparable to that of the formula for J_c^E based on Euler–Bernoulli beam theory, which is often recommended in the literature as a J-integral solution when LEFM is not valid (Biel and Stigh, 2007; 2008; Zhu et al., 2009; Banea et al., 2010). However, for higher values of μA_s, G_c^T would approach G_c^E, while J_c^E would approach J_c^T and Ω in Fig. 8(b).

Remark 4.3. Notice that in Fig. 8(b) $J_c^T = \Omega$, whereas $J_c^E \neq \Omega$, because the values of F and v used to compute the relevant curves

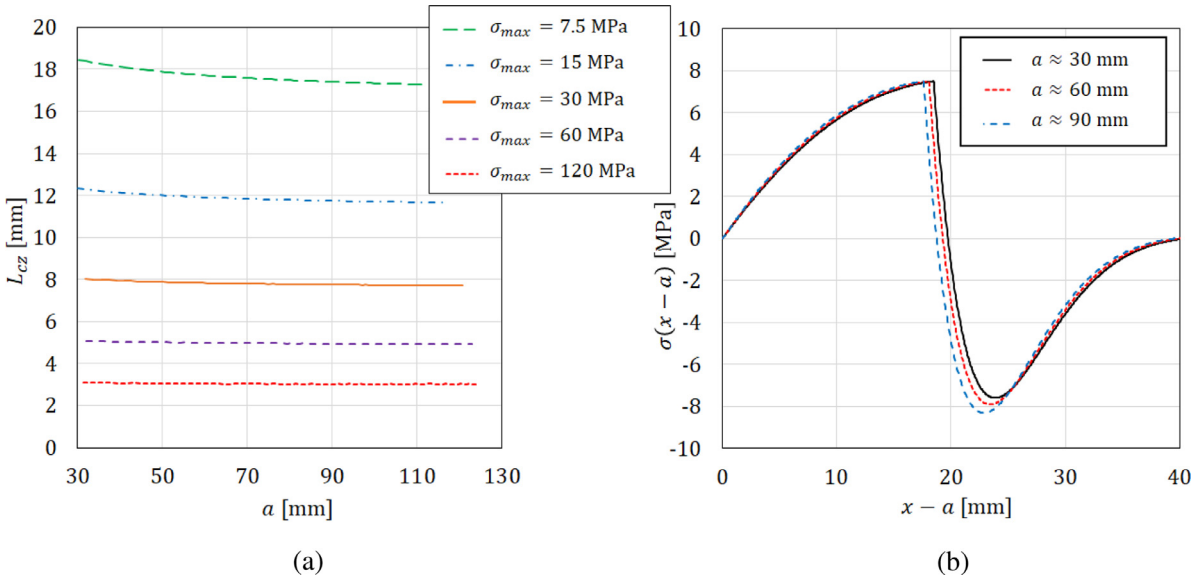

Fig. 9. Plots of (a) L_{CZ} for various values of σ_{max} and (b) interface traction distribution for three different crack positions for $\sigma_{max} = 7.5$ MPa.

are those obtained in the virtual experiment, in which Timoshenko beam theory was used. □

We define the cohesive-zone length, L_{CZ}, as the distance between the crack tip (the point separating the fully damaged from the partially damaged zone, where $\sigma = 0$) and the point on the interface where $\sigma = \sigma_{max}$. That is the zone of damage dissipation at the interface, whereas moving to the right from the peak tensile stress at the interface (where $\delta = \delta_0$) we enter the linear elastic zone where tensile stresses reduce as δ approaches zero. In this zone, proceeding further on in the rightward direction, at some point where $\delta = 0$ the interface stresses change from tensile to compressive. According to our CZM, however, no damage can occur in compression.

In Fig. 9(a) the decrease in L_{CZ} with crack propagation is shown for different values of σ_{max}, whereas in Fig. 9(b) the interface traction distribution corresponding to three different crack positions is shown for the most ductile case $\sigma_{max} = 7.5$ MPa. In the latter figure, the traction profile is shown with respect to the distance from the crack tip, $x - a$, to better appreciate how such profile changes with crack propagation.

From Fig. 9 it can be appreciated that both L_{CZ} and the traction profile are not constant with crack propagation, but their change is relatively very small. This is the case also for very ductile interfaces, i.e. for the smaller values of σ_{max}, for which the L_{CZ} are quite significant compared to the specimen dimensions. This indicates that, for all these cases, even for large values of L_{CZ}, the process is not exactly steady state but extremely close to being so.

The results presented confirm one of the fundamental results of this paper, expressed by Eq. (33): the accuracy of LEFM in predicting Ω does not depend on the size of the area of nonlinearity around the crack tip (i.e. L_{CZ}), but on how close the process is to steady-state, that is how close to zero is $d\Pi_D/da$ in (33).

This conclusion will be fully confirmed by the results presented in next section, for a DCB with prescribed rotations, in which crack propagation is indeed steady-state.

4.3. DCB with prescribed rotations

In this section, for the same set of parameters (see Tables 1 and 2), the results of virtual experiments are reported and discussed for the case in which the same DCB is loaded with prescribed rotations, as shown in Fig. 5(b). Denoting by v_θ the cross-head displacement due to a prescribed rotation θ, Fig. 10(a) shows that the applied moment M remains constant during crack propagation after reaching a certain critical value. This is perfectly in accordance with Eqs. (52) and (B.13) where it is obvious that the critical value of energy release rate G_c, which is equal to Ω, is obtained when moment $M = (\Omega\ b\ EI)^{1/2}$ is reached. In our case that value is $M = 28062.43$ Nmm.

Fig. 10(b) clearly shows that for each value of σ_{max}, the cohesive zone length L_{CZ} does not change during crack propagation, i.e. the process is steady-state. If we compare Figs. 10(b) and 9(a) we can see that, for each value of σ_{max}, L_{CZ} for the case of DCB with prescribed displacements approaches the values obtained for the same DCB with prescribed rotations as the crack propagates.

As expected, the values for G_c obtained from (52) for different σ_{max}, that is for any length of the cohesive zone, all match Ω, which on an extremely small scale can be seen in Fig. 11(a). Oscillations are again numerical artefacts dependent on the value of σ_{max}. In Fig. 11(b) we see that the derivative da_{eq}/da (where $a_{eq} = \theta\ EI/M$) also oscillates around the value of 1, but these results contain the additional error due to the 5-point numerical central differentiation used.

It is also useful to compare the cohesive-zone lengths for the considered values of σ_{max} with the length of one interface or beam element in our numerical model which is 0.1 mm. Even for the most brittle case L_{CZ} is approximately 30 times larger than the element length, so that the oscillation magnitude caused by the discretisation in the numerical solution is extremely small (see Fig. 11).

4.4. Rising R-curve

A variable fracture resistance (R-curve) could be due to a non-homogeneous interface. However, in most cases, and in particular when the fracture resistance is increasing with the crack advance, the R-curve is the result of progressive build-up of the actual dissipative phenomena at the microscale (Anderson, 1995). Nevertheless, the experimental characterisation of the fracture resistance in these cases is still typically obtained through the simple measurement of the R-curve, which implies lumping all the dissipative mechanisms into one single value of the energy. With this spirit, it

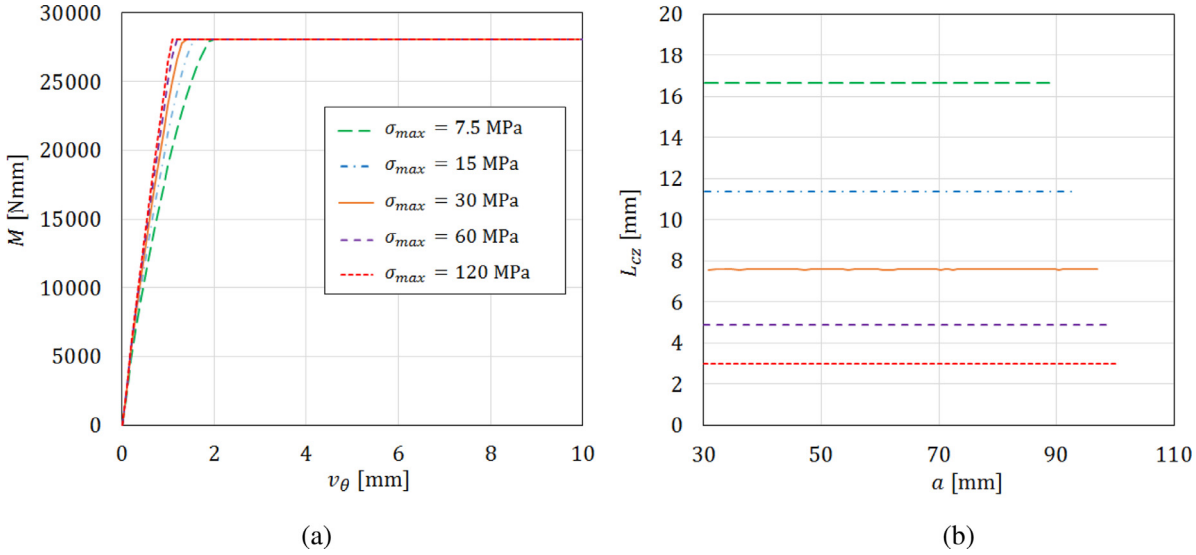

Fig. 10. DCB with prescribed rotations: (a) $M - v_\theta$ and (b) $L_{CZ} - a$ plots for various values of σ_{max}.

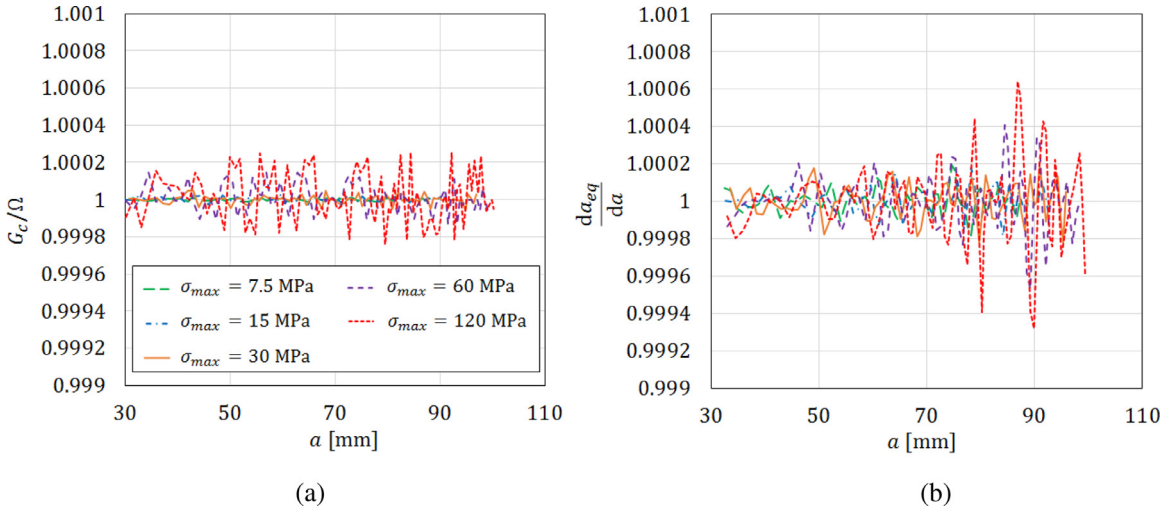

Fig. 11. DCB with prescribed rotations: (a) G_c/Ω and (b) da_{eq}/da for different values of σ_{max}.

makes sense that a numerical analysis based on a CZM considers variable input properties for the CZM to reproduce the R-curve.

Therefore, in this section we will address the case in which the traction-separation law is not the same along the interface. In particular, we will assume that the area under the curve, Ω, is increasing when moving away from the crack tip, starting from a value Ω_0 at the crack tip and asymptotically reaching a final value, Ω_∞, according to the following relationship, which is shown as a solid black line in Figs. 12–14:

$$\Omega(x) = \alpha(x)\,\Omega_\infty, \tag{58}$$

where the scaling factor α is given by

$$\alpha(x) = \frac{\Omega_0}{\Omega_\infty} + \left(1 - \frac{\Omega_0}{\Omega_\infty}\right)\left(1 - e^{-\frac{x-a_0}{c}}\right), \tag{59}$$

in which c is a 'decay length' and a_0 the initial crack length.

At all interface points a bi-linear CZM with the traction-separation law in Fig. 4 is again considered, but either one of σ_{max} and δ_c or both of them are assumed to vary along the interface. In particular, denoting by σ_∞ and $\delta_\infty = 2\,\Omega_\infty/\sigma_\infty$ the values of σ_{max} and δ_c corresponding to Ω_∞, we consider three cases, denoted as Cases A, B and C: in Case A, σ_{max} is kept constant, equal to σ_∞, and δ_c is scaled and therefore is taken equal to $\delta_c(x) = 2\,\Omega(x)/\sigma_\infty = \alpha(x)\delta_\infty$; in Case B, both σ_{max} and δ_c increase along x, scaled with respect to σ_∞ and δ_∞ by the same factor, which is therefore $\sqrt{\alpha(x)}$; in Case C, δ_c is kept constant, equal to δ_∞, and σ_{max} is scaled and therefore is taken equal to $\sigma_{max}(x) = 2\,\Omega(x)/\delta_\infty = \alpha(x)\sigma_\infty$. It is also assumed that $\delta_0 = 0.01\delta_c$ in all cases.

Table 3
Interface properties for the three cases with a rising R-curve.

Ω_0 [N/mm]	Ω_∞ [N/mm]	σ_∞ [MPa]	δ_∞ [mm]	c [mm]
0.5	1.0	30	1/15	20

The values of Ω_0, Ω_∞, σ_∞, δ_∞ and c are given in Table 3, whereas Table 4 provides a summary of the variations of σ_{max} and δ_c for the three cases.

Figs. 12–14 show the predicted values of the fracture resistance using the methods and formulae discussed in Section 3, compared to the values obtained using corrected beam theory (CBT) (BS ISO 25217:2009, 2009), G_c^{CBT}, and to the input value of the fracture resistance, Ω. CBT is added to this comparison because it appears to be the most reliable method available in the stan-

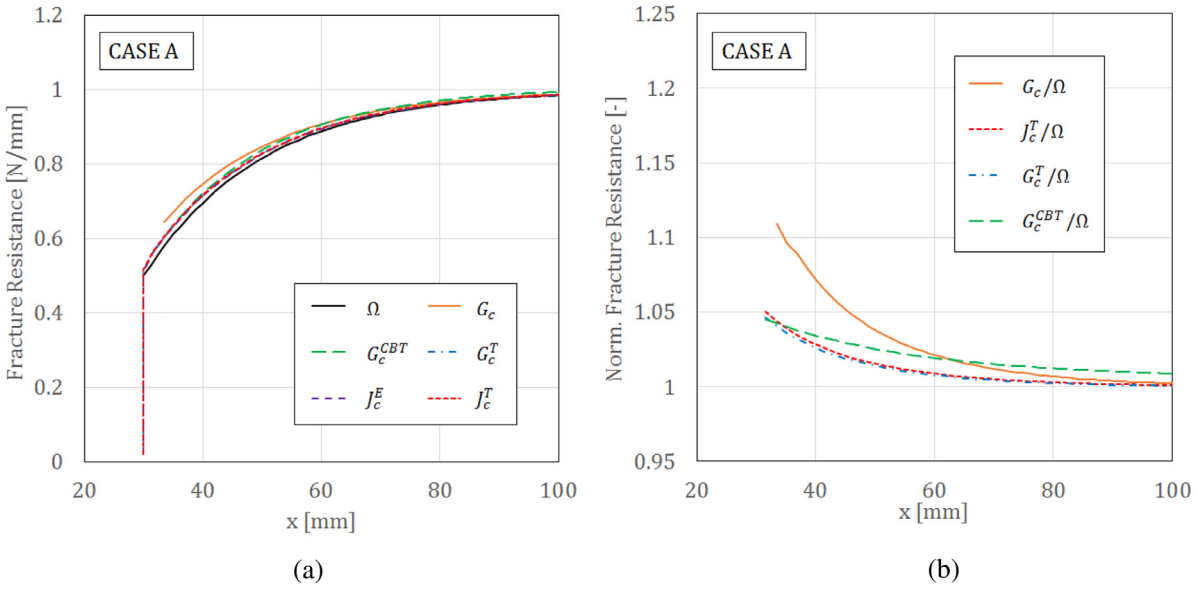

Fig. 12. Fracture resistance predictions for Case A: (a) actual values and (b) normalised values.

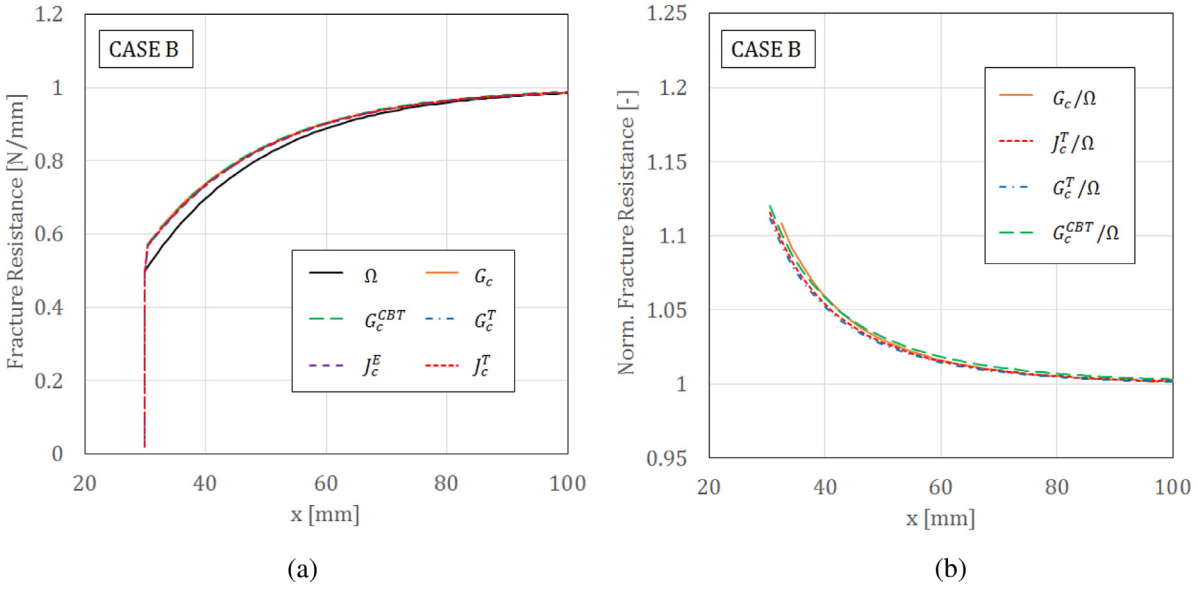

Fig. 13. Fracture resistance predictions for Case B: (a) actual values and (b) normalised values.

Table 4
Variations of σ_{max} and δ_c along the interface for the three different cases of a rising R-curve.

	$\sigma_{max}(x)$	$\delta_c(x)$
Case A	σ_∞	$\alpha(x)\,\delta_\infty$
Case B	$\sqrt{\alpha(x)}\,\sigma_\infty$	$\sqrt{\alpha(x)}\,\delta_\infty$
Case C	$\alpha(x)\,\sigma_\infty$	δ_∞

dards (ASTM D5528, 2013), as will be confirmed by our results in Section 5. To compute G_c^{CBT}, Eq. $(60)_2$ is used, where the crack length correction $\overline{\Delta}$ is obtained as explained in BS ISO 25217:2009 (2009). The curve for G_c^E is not reported but it is at all points within less than 1% of the one obtained for G_c^T.

On the right-hand side of each figure the same predictions at each point x normalised with respect to $\Omega(x)$ are reported to better appreciate the discrepancy. Note that, predictions for G_c start from values of x greater than a_0, because they require the use of the derivative da_{eq}/da, which is computed by finite differences and only when the crack has started propagating.

At any point x of the interface, all methods predict a value of the fracture resistance which is less close to the input value $\Omega(x)$ if compared with the predictions given in the case of a flat R-curve. This can be expected for the accurate value of the critical energy release rate, G_c, that is the value that is obtained by taking into account the derivative da_{eq}/da via either Eq. (42) or Eq. (44) (which again give the same value). The reason is that, because of the increase of $\Omega(x)$ as the crack propagates along the interface, the term $d\Pi_D/da$ in Eq. (33) is positive. This results in a discrepancy between G_c and Ω that is between 10% and 15% at the start of the crack propagation, and quickly decreases to values less than 5%. The biggest discrepancy is for Case A, which is in fact the least ductile, and the lowest discrepancy is for Case C, which is the most ductile.

It is interesting to observe that the effect of the derivative da_{eq}/da is much higher for Cases A and C than for Case B, which

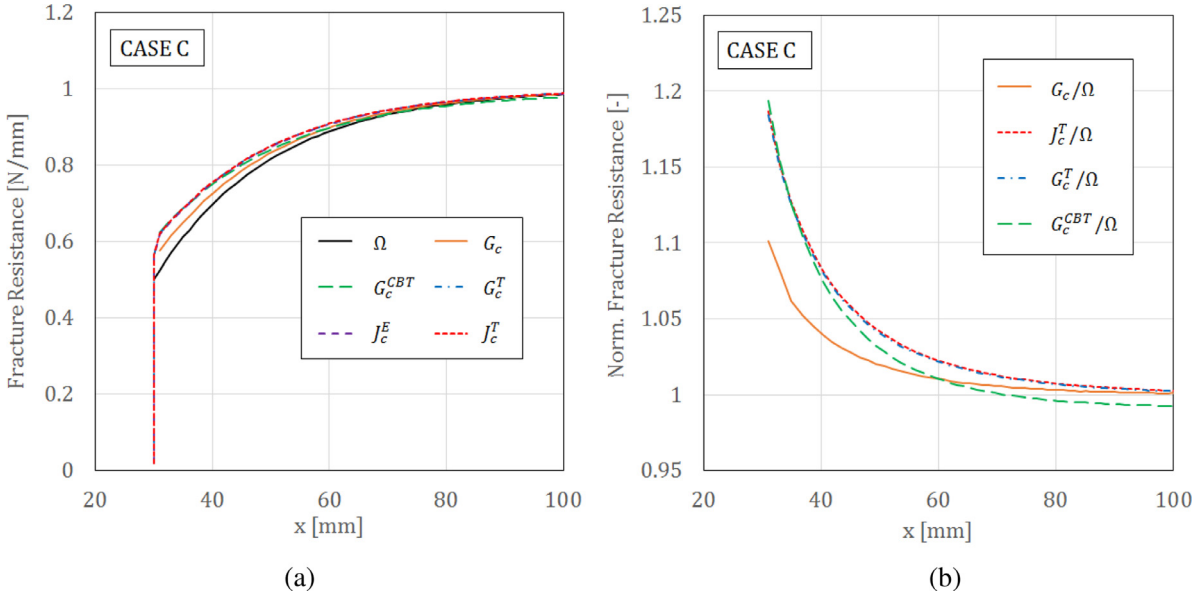

Fig. 14. Fracture resistance predictions for Case C: (a) actual values and (b) normalised values.

Table 5
Percentage discrepancy between $-(1/b)\,(\Pi_{NL}(a_0+\Delta a)-\Pi_{NL}(a_0))$ and the integral of Ω between the same limits, for $\Delta a = 1$ mm and for two values of the prescribed displacement increments, Δv.

Δv [mm]	Case A	Case B	Case C
0.1	1.18%	−1.78%	−1.24%
0.01	−0.01%	−0.01%	−0.01%

explains the larger difference between G_c^T (and G_c^E, not reported) and G_c for Cases A and C with respect to the discrepancy in Case B. This can be explained because the length of the cohesive zone, L_{CZ}, can be approximately taken to be proportional to Ω/σ_{max}^2 (Turon et al., 2007), which in Case B would lead to a constant value of L_{CZ}. Clearly, this is an approximation because we have seen that the process is not steady-state and L_{CZ} still varies, but its variation is very limited as in the case of a flat R-curve. In turn, this makes the derivative da_{eq}/da of the same order of magnitude as for the case of a flat R-curve, which is very small.

The predictions of G_c^T and J_c^T appear all very close to each other. In fact, their maximum difference is of the order of 1–2%, for the shortest crack lengths, which is very close to that found for the case of a flat R-curve. Because the total discrepancy with respect to Ω is larger here than in the case of a flat R-curve (e.g. Fig. 8), one can appreciate from Figs. 12–14 that the predictions provided by G_c^T and J_c^T are effectively the same, which is a very important result form an engineering point of view.

The discrepancy between J_c^T and Ω can be explained because the interface is not homogeneous. Therefore, as discussed in Section 2.3 (see Remark 2.1), this results in $J_c \neq \Omega$.

CBT provides predictions of the fracture resistance which are close to those given by G_c^T and J_c^T, although for cases A and C, for increasing crack lengths, G_c^{CBT} does not tend to Ω, whereas G_c^T and J_c^T do. The values of the correction $\overline{\Delta}$ determined in the CBT are equal to 8.25, 9.00 and 10.26 mm, for Cases A, B and C.

Although here J_c^T is not equal to the so-called nonlinear energy release rate, given by $-(1/b)\,\partial\Pi_{NL}/\partial a$, the latter is still equal to the work of separation, Ω, in accordance with Eq. (19). Because of the variation of Ω with x and the numerical noise occurring with very small crack advances Δa, Eq. (19) is here validated by numerically computing the change, $-(1/b)\,(\Pi_{NL}(a_0+\Delta a)-\Pi_{NL}(a_0))$, from the FE solution, and comparing it with the integral of function Ω of Eq. (58) for the same region. The discrepancy in percentage is reported in Table 5 for $\Delta a = 1$ mm and for two different values of the constant prescribed displacement increments. For the more refined time-discretisation it is clear that the error becomes negligible.

The effect of the non-homogeneity of the interface is also that the derivative of the J integral with respect to the crack-tip opening, δ_{CT} does not provide the traction-separation law, which makes this identification method not strictly valid. This is shown numerically in Fig. 15. In particular, Fig. 15(d) shows that, in the case of a flat R-curve, namely with $\Omega = \Omega_\infty$, $\sigma_{max} = \sigma_\infty$ and $\delta_c = \delta_\infty$ for all x, the numerically computed value of $dJ_c^T/d\delta_{CT}$ is exactly equal to the stress σ.

Remark 4.4. Considering the effect that different ways to vary σ_{max} and δ_c have on the results presented in this section, it is reasonable to deduce that the whole shape of the traction-separation law can influence the accuracy of the predictions. Therefore, the numerical results presented here are very useful to support some of the theoretical results obtained in Sections 2 and 3, but they cannot be considered as a comprehensive analysis of the case where a significant R-curve is found from experimental testing.

On the other hand, from the results presented in this section one can already conclude that J-integral predictions, which require the difficult measurement of rotations, are not more accurate than the formulae for G_c^E or G_c^T, which are based on LEFM and do not require the measurement of the crack length (unlike CBT) or rotations.

It is also worth noting that the results have been presented here in the form of curves showing the fracture resistance against interface position, x, where x is effectively the crack length. The latter is not to be measured to obtain G_c^E or G_c^T, so the actual calculation of G_c^E or G_c^T can only be made against a_{eq}. However, in most practical situations, knowledge of the fracture resistance at a specific point of the interface is not really needed, whereas the actual

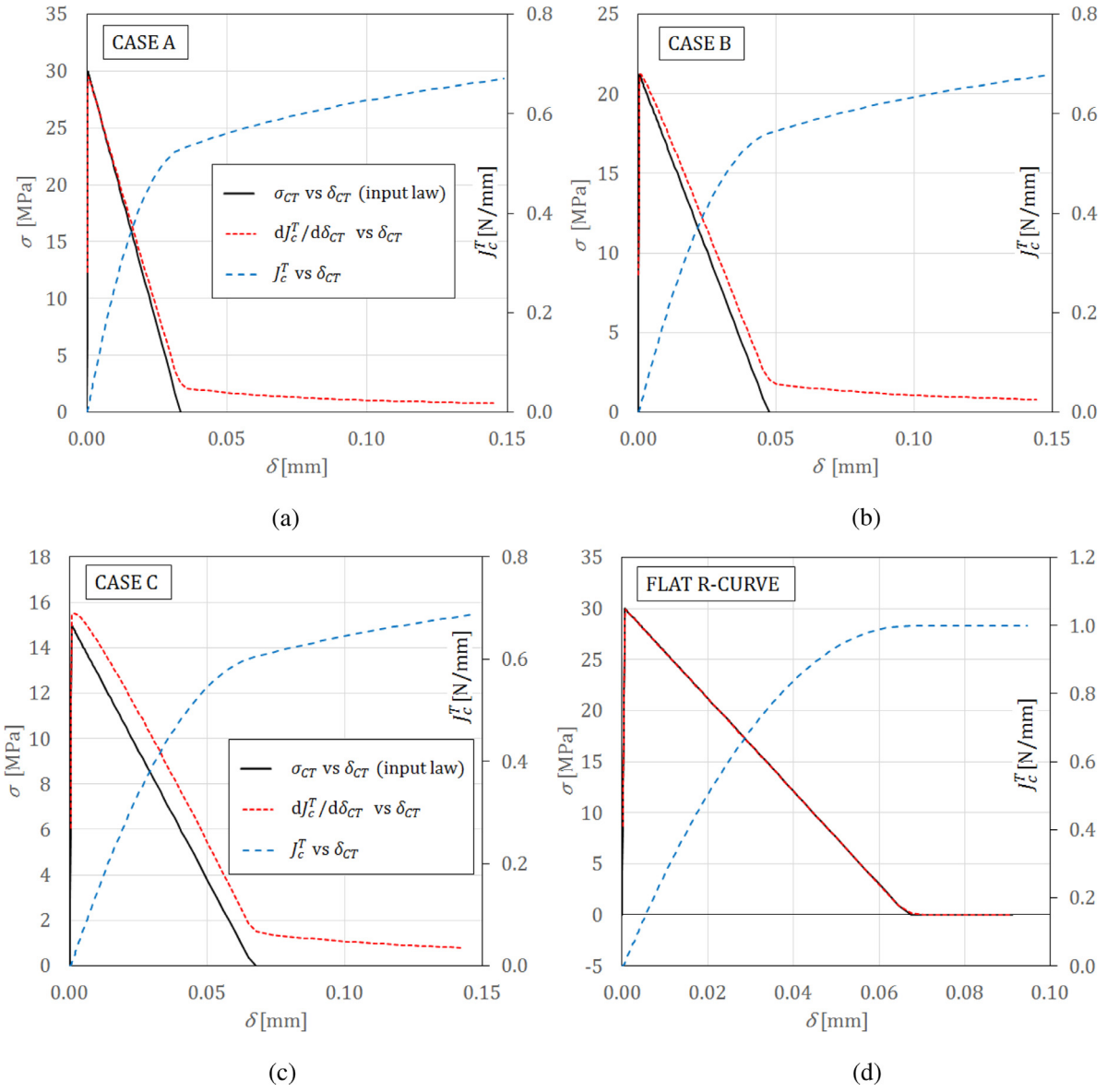

Fig. 15. Comparison between the interface stress and $dJ_c^T/d\delta_{CT}$ for (a) Case A, (b) Case B, (c) Case C and (d) for the case of a flat R-curve.

initiation and the so-called 'steady-state' (i.e. asymptotic) values of the fracture resistance are important.

5. Comparison of LEFM and formulae for G_c used in standards on real experiments

To perform the DCB virtual experiments in the previous sections we have used realistic material and geometrical properties for the DCB arms and the adhesive, for a number of values of σ_{max} and with $\Omega = 1$ N/mm kept constant. We have shown that for the cases analysed, the input value of Ω can be accurately predicted using the analytical formulae based on LEFM. In this section we will additionally demonstrate that G_c^E and G_c^T provide very accurate predictions of Ω for a wide range of specimen dimensions and materials as well as for adhesives with different values of Ω. Furthermore, we will show that this accuracy is normally comparable or even higher than that provided by the methods used in BS ISO 25217:2009 (2009).

Three different examples are used, all based on experimental measurements from the literature. The first example is the CFRP DCB delamination test studied by Blackman et al. (2003a). By using a FE model, they have fitted the experimental measurements with a cubic polynomial $\sigma - \delta$ CZM law and determined the values $\Omega = 0.257$ N/mm and $\sigma_{max} = 50$ MPa. The second example is a DCB made of aluminium adherents and bonded with the epoxy adhesive Hysol® 9466, and is taken from the paper by Alfano et al. (2011), where a trapezoidal constitutive law was used in the CZM and values $\Omega = 2.7$ N/mm and $\sigma_{max} = 14$ MPa were determined again by fitting the experimental measurements. Although in our model a bi-linear constitutive law is used for the CZM, using the CZM parameters determined in Blackman et al. (2003a) and Alfano et al. (2011) can be justified, especially in the crack propagation phase where Ω is the most important CZM parameter. The last example, presented by Lopes et al. (2016), is a DCB made of steel adherends bonded with the epoxy adhesive Hysol® 7752, which has not involved any numerical modelling and the value of G_c has been obtained using simple analytical formulae. The compliance-based beam method (CBBM), introduced in the same paper, has been taken to give the best prediction of $G_c = 4.5$ N/mm, which is adopted as Ω in our

Table 6
Data used in the set of virtual experiments based on real ones.

Experiment	Adherends	Adhesive	L [mm]	h [mm]	b [mm]	a_0 [mm]	E [GPa]	Ω [N/mm]	σ_{max} [MPa]	FEs per arm
1	CFRP	Hysol® 9309	110	1.55	24	22	137	0.257	50	2200
2	Aluminium AA6060-TA16	Hysol® 9466	200	15	25	30	65.7	2.7	14	2000
3	Steel C45E	Sikaforce® 7752	300	12.7	25	55	204	4.5	15	3000

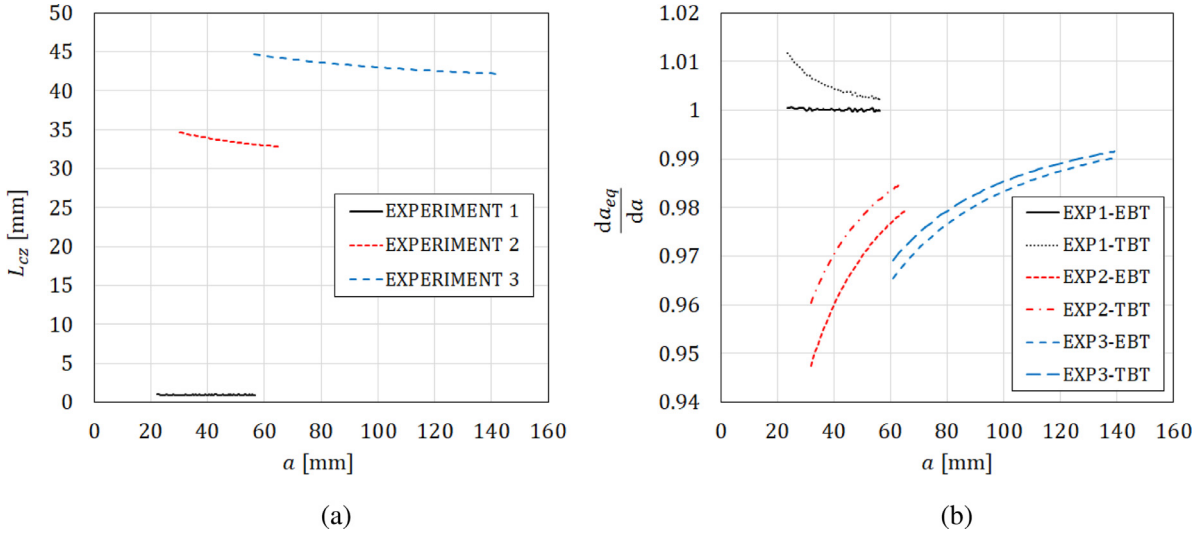

Fig. 16. Values of (a) L_{CZ} and (b) da_{eq}/da (both for EBT and TBT) for three different real DCB experiments.

numerical model. We additionally determined the value $\sigma_{max} = 15$ MPa by fitting the experimental $F-v$ curve. All the relevant data used in this set of virtual experiments is presented in Table 6.

In the bi-linear CZM used in the present analysis, $\delta_c = 2\Omega/\sigma_{max}$ and $\delta_0 = 0.01\delta_c$ for all adhesives. The virtual experiments are performed by prescribing the displacement, v, up to the maximum values, which approximately correspond to those reported in Blackman et al. (2003b), Alfano et al. (2011) and Lopes et al. (2016).

These case studies cover a wide range of adhesive behaviours, from extremely brittle, to extremely ductile. This can be seen in Fig. 16(a), where for Experiment 1 the length of cohesive zone $L_{CZ} \approx 1$ mm, while for the other two examples we have cohesive-zone lengths which are definitively large compared to the specimen dimensions. The derivatives da_{eq}/da for Euler–Bernoulli (EBT, $a_{eq} = a_{eqE}$) and Timoshenko (TBT, $a_{eq} = a_{eqT}$) beam theory are shown in Fig. 16(b), which again demonstrates that crack propagation is not steady-state.

In Figs. 17–19, the accuracy of the various data reduction schemes in predicting the input value Ω used in our numerical model is shown. Since for each experiment we have a different value of Ω, values of G_c obtained using different approaches are normalised with respect to the corresponding value of Ω.

On the left-hand side of Figs. 17–19, the fracture resistance determined with the data reduction schemes used in BS ISO 25217:2009 (2009) are compared. They are namely simple beam theory (SBT), corrected beam theory (CBT) and experimental compliance method (ECM) and they evaluate G_c according to the following expressions:

$$G_c^{SBT} = \frac{4F^2}{Eb^2}\left(\frac{3a^2}{h^3} + \frac{1}{h}\right), \quad G_c^{CBT} = \frac{3Fv}{2b(a+\overline{\Delta})}, \quad G_c^{ECM} = n\frac{Fv}{2ba}. \tag{60}$$

Note that the expression for G_c^{SBT} can be obtained from Eq. (47) by assuming that the material of the arms is isotropic with $\nu = 1/3$, $k_s = 2/3$, and, more importantly, by incorrectly assuming that a is equal to a_{eqT}. The term $\overline{\Delta}$ in expression for G_c^{CBT} represents a crack length correction which is obtained graphically from the $\log a - \log C^{1/3}$ plot, where $C = v/F$ is the measured compliance. Factor n in expression for G_c^{ECM} is the slope of the linear fit of the $\log a - \log C$ data and is also obtained graphically. Note that all the methods from this standard require the measurement of the crack length a. More details about these methods can be found in BS ISO 25217:2009 (2009).

Among the considered standards, CBT proves to be the most accurate data reduction scheme, ECM does not provide satisfactory accuracy, while SBT gives substantial errors. On the other hand, on their right-hand sides, Figs. 17–19 show that G_c^E, G_c^T and G_c predict the values of fracture resistance that have either similar or better accuracy than those given by CBT. Since to compute the derivative in formulae (42) or (44) for G_c, the crack length measurement is required, we do not consider these data-reduction formulae for G_c to be practical enough. On the other hand, formulae (45) for G_c^E and G_c^T, which do not require crack length measurement, provide extremely accurate predictions of Ω in all the cases considered, even for extremely ductile cases (see Fig. 19(b)). In Figs. 18 and 19 we show that these formulae can indeed be more accurate even than CBT, which requires measurement of the crack length. The only exception is the CFRP DCB delamination test (Experiment 1), for which the response is almost brittle and, as shown in Fig. 17(b), G_c^T gives a slightly worse prediction than the other methods. This is however expected since in Section 4.2 we have already explained why G_c^T does not converge to Ω for brittle CZMs ($\sigma_{max} \to \infty$).

Remark 5.1. Because of the rapidly decreasing discrepancy between G_c^E or G_c^T and Ω with increasing crack propagation, numerical analyses similar to ones presented in this article could be conducted for a wider range of cases of industrial interest to identify optimal dimensions of the specimen (h and L) and of the initial crack length, a_0, which, for given adhesive and bulk material, give the best estimation of Ω using formulae (45) for G_c^E or G_c^T, by reducing the discrepancy in the early phase of crack propagation.

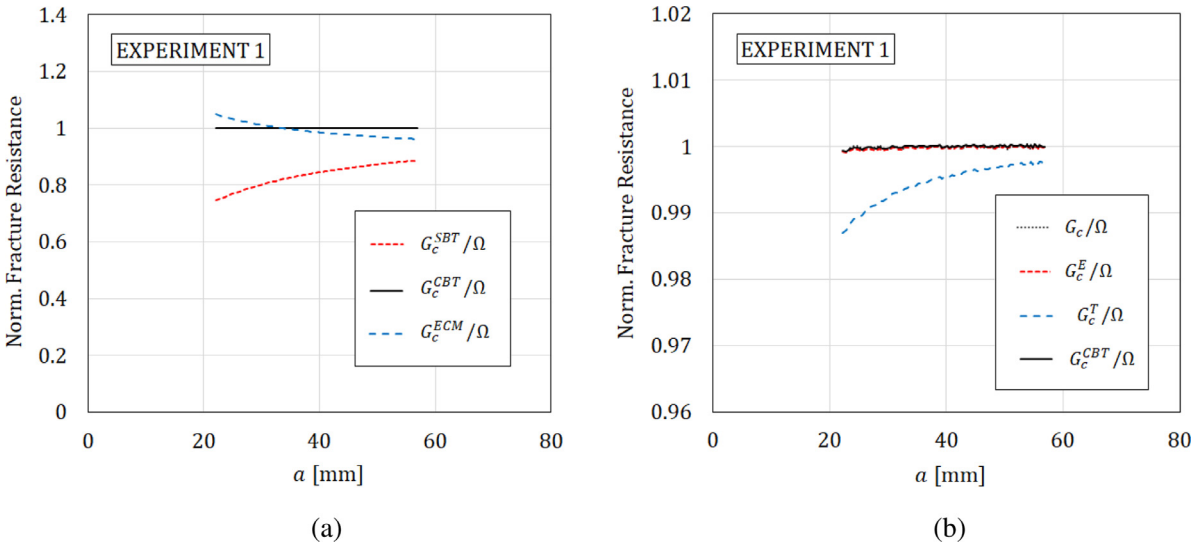

Fig. 17. Normalised values of (a) G_c^{SBT}, G_c^{CBT} and G_c^{ECM}, and (b) G_c^{CBT}, G_c^{E}, G_c^{T} and G_c for a CFRP DCB (Blackman et al., 2003a).

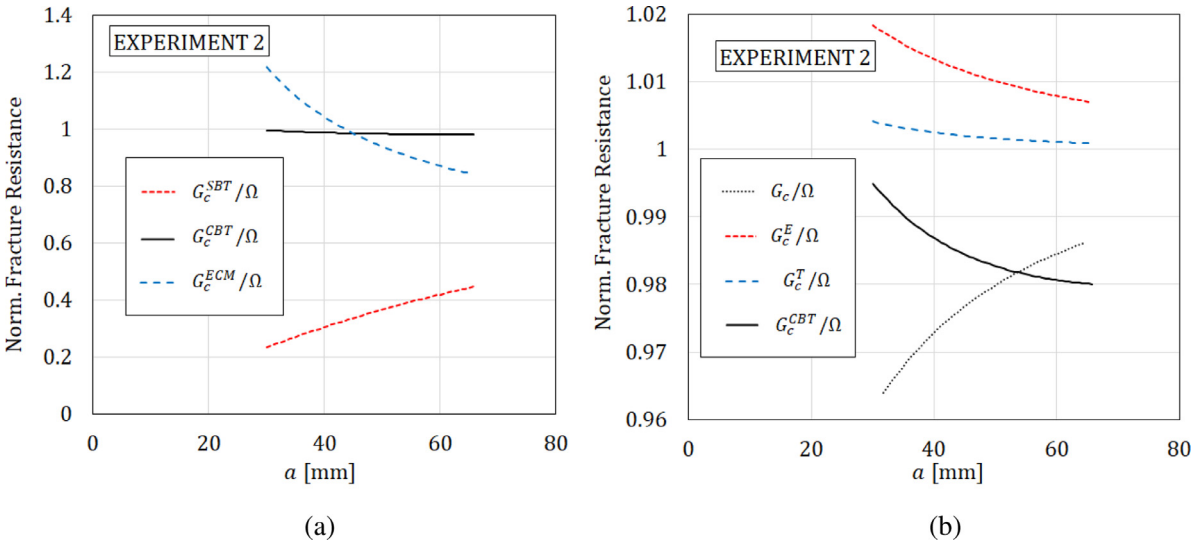

Fig. 18. Normalised values of (a) G_c^{SBT}, G_c^{CBT} and G_c^{ECM}, and (b) G_c^{CBT}, G_c^{E}, G_c^{T} and G_c for a DCB with aluminium arms and epoxy adhesive (Alfano et al., 2011).

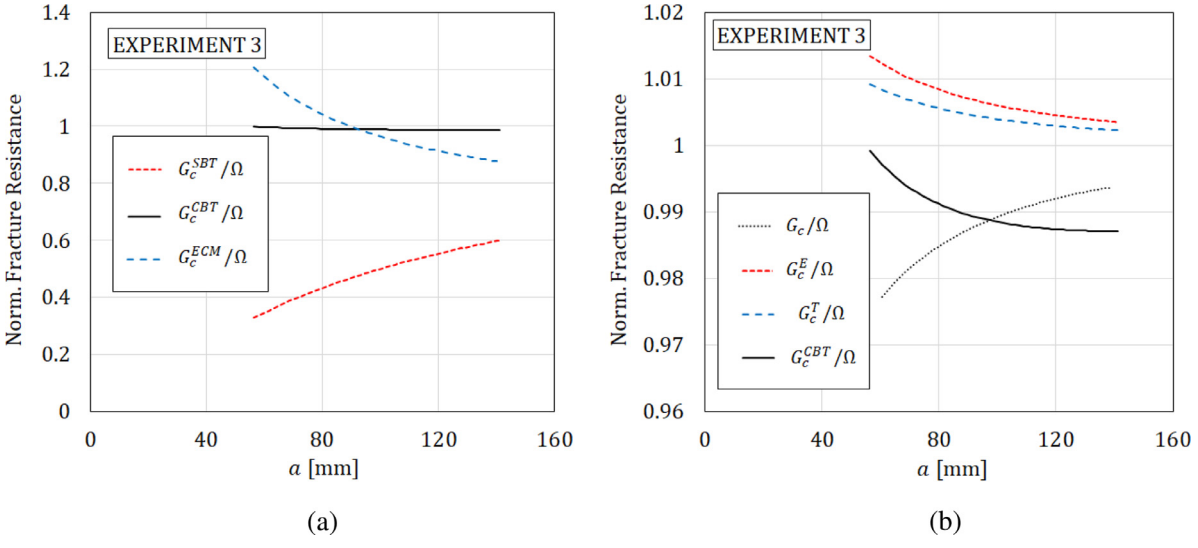

Fig. 19. Normalised values of (a) G_c^{SBT}, G_c^{CBT} and G_c^{ECM}, and (b) G_c^{CBT}, G_c^{E}, G_c^{T} and G_c for a DCB with steel arms and epoxy adhesive (Lopes et al., 2016).

6. Conclusions

In this paper, we have reviewed and partly revised fundamental concepts of fracture mechanics, we have provided new and more rigorous theoretical derivations of formulae proposed in the literature for the experimental determination of fracture resistance without measuring the crack length and we have reported and discussed extensive numerical analyses to support our theoretical arguments. The focus has been the characterisation of the fracture resistance of thin quasi-brittle interfaces undergoing damage and failure in mode I, between two parts of a body that behave elastically, which is the typical case considered when characterising the fracture resistance of adhesive joints or the delamination resistance of FRP laminates.

The results obtained can be more clearly summarised by separating them into one set of conclusions with immediate and significant practical relevance for engineers in the industry and a second set, with the conceptual novelties contributed and the open issues which remain to be addressed or are indeed raised by this work.

6.1. Summary of results of practical interest for engineers

The following conclusions can be drawn and recommendations made based on the results obtained:

- The DCB with prescribed displacements is the recommended test to be conducted, because not only are specimens easily prepared, fixtures straightforward and a conventional testing machine needed, but also because very accurate predictions of the work of separation, Ω, can be obtained with formula (46) for G_c^E and (47) for G_c^T, both based on LEFM, which do not require the measurement of the crack length or of the end rotations. Formula (46) for G_c^E has the advantage of not requiring the measurement of the shear modulus.
- For significantly rising R-curves, the results presented indicate that G_c^E and G_c^T provide as accurate predictions of the fracture resistance as the most accurate data-reduction scheme currently recommended in the standards.
- CBT, which is the most accurate method in the current standards, has the advantage that material and geometrical properties are not needed. However, the uncertainty related to the measurement of the crack length are much higher than that those associated with the measurement of the geometrical dimensions. As for the material properties, the effective Young's modulus is required for the computation of G_c^E and G_c^T, and can indeed vary with respect to the uniaxial modulus because of constraints on the anticlastic bending. However, this effect can be taken into account by one-off analyses for different cross section dimensions and rig fixtures, which could be incorporated in a new standard. Furthermore, these analyses could be avoided or at least complemented with 'post-mortem' 3-point bending tests made on the two arms of the DCB specimens (i.e. once they have been separated from each other).

6.2. Summary of results in terms of fundamental concepts

We have shown that the widely accepted principle that LEFM cannot be used in presence of large areas of nonlinearity is not generally true. For the problems addressed in this article, which are mode-I debonding of adhesive joints or delamination of composites, this means that even in presence of a large cohesive zone, the critical energy release rate, G_c, determined using LEFM-based methods, is extremely close to the work of separation, Ω, required to separate two infinitesimal areas of the interface, that is the area under the traction-separation law if a CZM is used.

Therefore, the difference between G_c and Ω does not depend on the size of the cohesive zone, as mostly stated in the literature so far, but it depends on the extent by which the dissipation process does not advance in a steady-state fashion.

Indeed, when the profile of the specific dissipation in front of the crack tip advances in a steady-state way, like in the case of a DCB with prescribed rotations with constant properties on the interface, there is no difference between G_c and Ω.

For a DCB with prescribed forces, the process is not steady-state but it is very close to being so, at least in the case of a flat R-curve, i.e. when the fracture resistance does not change with crack propagation. This explains the great accuracy of LEFM-based methods in predicting Ω also in presence of large cohesive zones.

In case of a flat R-curve, Ω turns out to be equal to the critical J integral, J_c. Therefore, in this case our analysis provides a clear relationship between G_c and J_c, shedding light on a long debate about which one of these two parameters should be used to characterise fracture resistance.

For a non-flat R-curve, the fracture resistance is found to vary (typically increase) with the advance of crack propagation. Unless the actual dissipation phenomena leading to such R-curve are separately modelled, a non-flat R-curve is effectively equivalent to have non-homogeneous interface with Ω varying in the direction of crack propagation. In such case, we have shown that $J_c \neq \Omega$, which has never been pointed out in the literature. This also implies that the derivative of the J integral with respect to the crack-tip displacement does not provide the exact traction-separation law, although it is still a useful approximation of it that also gives insight into the shape of the law.

In order to determine G_c, we have shown that the methods so far proposed that do not require the measurement of the crack length did not take into account the conceptual difference between the so-called equivalent length, a_{eq}, and the actual crack length, a. The expression for G_c used in these methods should be multiplied by the derivative $\mathrm{d}a_{eq}/\mathrm{d}a$, whose knowledge however would again require the measurement of the crack length.

On the other hand, we have shown in our numerical results, for a wide range of cases of practical interest, that $\mathrm{d}a_{eq}/\mathrm{d}a$ is indeed very small for a flat R-curve in a DCB tested with prescribed forces, again because the process is close to being steady-state. For this reason, the values predicted by these methods, denoted by G_c^E and G_c^T, when the Euler–Bernoulli or Timoshenko theories are used, respectively, are extremely close to G_c. For a significantly rising R-curve, the difference between G_c and G_c^E or G_c^T can be not negligible for short crack lengths but it becomes negligible for sufficiently large crack lengths.

6.3. Future work

Although in this paper we have studied problems covering a wide range of cases of engineering interest, more numerical work and possibly the creation of a database of numerical results can be very helpful to provide even more robust estimates of the accuracy of all methods investigated in this paper. It will also be very useful to accompany this benchmarking exercise with a wide range of experimental tests, possibly within the context of a round robin, to appreciate how much measurement errors and scatter of material and geometrical properties contribute to the discrepancies in addition to those considered in this paper, which are only due to the actual data-reduction scheme used.

Supplementary data

Supplementary material related to this article can be found online at http://dx.doi.org/10.17633/rd.brunel.6194483.

Acknowledgements

This project has received funding from the European Union's Horizon 2020 research and innovation programme under the Marie Sklodowska-Curie grant agreement No. 701032. The third author wishes to acknowledge the financial support of the Croatian Science Foundation (Research Project IP-2016-06-4775).

Appendix A. Derivation of a closed-form expression for J_c^T

The J integral of Eq. (20) is here given by:

$$J = \int_\Gamma \left(w\, n_x - t_y \frac{\partial u_y}{\partial x} \right) \mathrm{d}s \tag{A.1}$$

because $t_x = 0$. Considering the contour Γ (line *ABCDEG*) shown in Fig. A1, the only part of Γ where both w and n_x are not zero are the two straight lines *AB* and *EG*, where for the case of Timoshenko beam theory the strain energy is only due to the shear stresses and strains, which are to be assumed constant and equal to F/A and $F/(\mu A_s)$, respectively. So it results:

$$\begin{aligned} \int_\Gamma w\, n_x \,\mathrm{d}s &= \int_A^B \frac{F^2}{2\,\mu A_s A}\,\mathrm{d}y + \int_E^G \frac{F^2}{2\,\mu A_s A}\,\mathrm{d}y \\ &= 2\int_0^{-h} \frac{F^2}{2\,\mu A_s A}\,\mathrm{d}y = \frac{F^2}{b\,\mu A_s A}\int_0^{-h} b\,\mathrm{d}y = -\frac{F^2}{b\,\mu A_s} \end{aligned} \tag{A.2}$$

For the second term of the integral, the reaction forces where displacements are prescribed are approximated here as concentrated forces, which means that the tractions t_y can be considered applied on infinitesimal areas where $\partial u_y/\partial x$ is constant (and can be taken out of the integral in (A.1) . As we have denoted by θ_v the rotation of the top arm where the displacement is prescribed, assumed positive if anti-clockwise, one has:

$$\text{Top: } \frac{\partial u_y}{\partial x} = \theta_v - \frac{F}{\mu A_s} \qquad \text{Bottom: } \frac{\partial u_y}{\partial x} = -\theta_v + \frac{F}{\mu A_s} \tag{A.3}$$

Since $\partial u_y/\partial x$ can be taken out of the integral, whereas t_y is positive on the top and negative on the bottom, one has

$$\int_\Gamma t_y \frac{\partial u_y}{\partial x}\,\mathrm{d}s = 2\left(\theta_v - \frac{F}{\mu A_s}\right)\frac{1}{b}\int_{\Gamma^*_{top}} t_y\, b\,\mathrm{d}s = \frac{2}{b}\left(F\,\theta_v - \frac{F^2}{\mu A_s}\right) \tag{A.4}$$

where Γ^*_{top} is the infinitesimal area on the top where tractions are applied.

Replacing Eqs. (A.2) and (A.4) into Eq. (A.1), one finally obtains:

$$J = \frac{F^2}{b}\left(\frac{1}{\mu A_s} - \frac{2\,\theta_v}{F}\right) \tag{A.5}$$

which has been denoted by J_c^T in Eq. (54) to indicate that it is derived according to Timoshenko beam theory and because in that equation the critical value of the J integral is considered, i.e. during crack propagation.

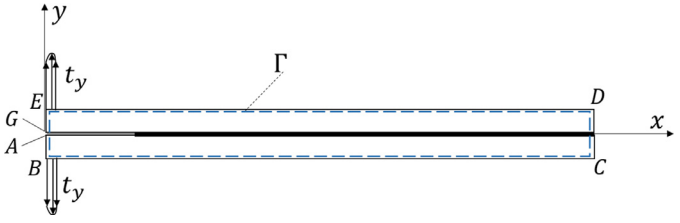

Fig. A1. J-integral contour Γ used to determine J_c^T.

Appendix B. Determination of Ω for a DCB specimen via solution of beam differential equations

For a DCB with prescribed displacement or rotations, using simple beam theories we can find exact analytical formulae for the work of separation, Ω, i.e. the area under the traction-separation law of the CZM, assuming that the interface properties, including Ω, are constant along the interface. A similar approach was proposed in Olsson and Stigh (1989) for Euler–Bernoulli beam theory. Here we also derive the expressions for Timoshenko beam theory for a DCB with either displacement or rotations prescribed.

Let us consider a Timoshenko beam representing the upper arm of a DCB with interface tractions $\sigma(x)$ as shown in Fig. B1.

We note that the origin of the coordinate system is located at the crack tip, which is the point where the relative displacement $\delta(0) = \delta_c$. Due to symmetry, $\delta(x) = 2\,u_y(x)$, where $u_y(x)$ is the displacement of the upper layer in the y-direction. The distribution of interface tractions over the beam length, $\sigma(x)$, will depend on the shape of the traction-separation law, $\sigma(\delta)$, and on the boundary conditions, i.e. whether we apply force, F, or moment, M, at $x = -a$. In Fig. B1 we consider a general case, where the relationship $\sigma(\delta)$ does not need to be defined *a priori*, so that this proof is valid for any type of CZM. The segment of the DCB arm that is completely separated does not enter the observed domain ($x \in [0, \infty)$), but is taken into account by the boundary conditions at $x = 0$.

According to Timoshenko beam theory, we have

$$EI\, u_y^{IV}(x) + \frac{EI}{\mu A_s} q''(x) = q(x), \tag{B.1}$$

where distributed load $q(x)$ according to Fig. B1 can be written as $q(x) = -\sigma(x)\ b$ and the derivatives are total derivatives with respect to x.

By multiplying the entire equation by $u_y'(x)$ and integrating over x from 0 to ∞, we obtain

$$\begin{aligned} EI\int_0^\infty u_y^{IV}(x)u_y'(x)\mathrm{d}x + \frac{EI}{\mu A_s}\int_0^\infty q''(x)u_y'(x)\mathrm{d}x \\ = -b\int_0^\infty \sigma(x)u_y'(x)\mathrm{d}x. \end{aligned} \tag{B.2}$$

Solving the integral on the right-hand side,

$$\int_0^\infty \sigma(x)u_y'(x)\mathrm{d}x = -\int_0^{\delta_c/2}\sigma(u_y)\mathrm{d}u_y = -\frac{1}{2}\Omega,$$

gives the work of separation Ω. To solve the integrals on the left-hand side we integrate by parts and using relations

$$q(x) = \mathcal{T}'(x), \tag{B.3}$$

$$\mathcal{T}(x) = \mathcal{M}'(x) = EI\,\varphi''(x) = EI\,u_y'''(x) + \frac{EI}{\mu A_s}q'(x), \tag{B.4}$$

where $\mathcal{T}(x)$, $\mathcal{M}(x)$ and $\varphi(x)$ are the cross-sectional shear force, bending moment and rotation functions, we obtain

$$\begin{aligned} \int_0^\infty u_y^{IV}(x)u_y'(x)\mathrm{d}x &= \left[u_y'(x)u_y'''(x) - \frac{1}{2}u_y''(x)^2\right]_0^\infty, \\ \int_0^\infty q''(x)u_y'(x)\mathrm{d}x &= \left[u_y'(x)q'(x) - q(x)u_y''(x) + \frac{1}{2EI}\mathcal{T}(x)^2\right. \\ &\quad \left. - \frac{1}{2\mu A_s}q(x)^2\right]_0^\infty. \end{aligned} \tag{B.5}$$

Expressions (B.5) are then substituted in Eq. (B.2) which, after substituting $q'(x)$ from (B.4) and $q(x)$ from

$$\mathcal{M}(x) = EI\,u_y''(x) + \frac{EI}{\mu A_s}q(x), \tag{B.6}$$

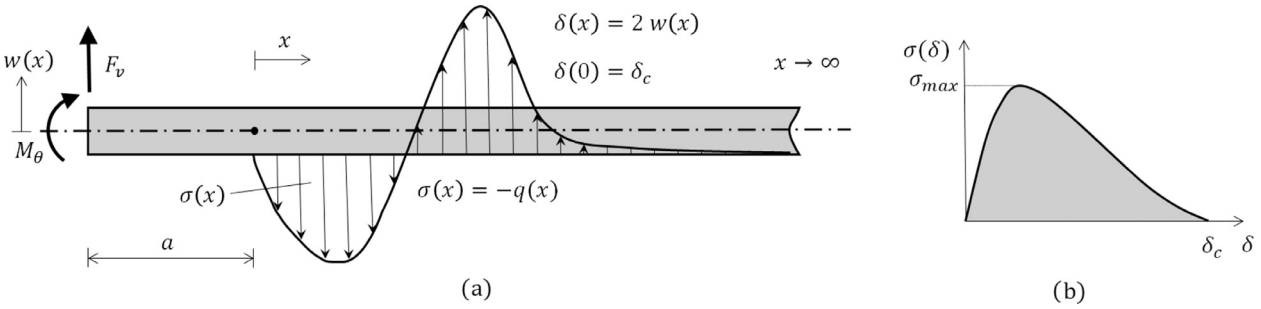

Fig. B1. Analytical model for a DCB: (a) Timoshenko beam representing the upper arm with interface tractions and (b) traction-separation law at the interface.

simplifies to

$$\left[\varphi(x)\ \mathcal{T}(x) - \frac{\mathcal{T}(x)^2}{2\mu A_s} - \frac{\mathcal{M}(x)^2}{2EI}\right]_0^{\infty} = \frac{b}{2}\Omega. \tag{B.7}$$

From Eq. (B.7), Ω can be determined for different boundary conditions at the crack tip ($x = 0$) and at the end of the specimen ($x = \infty$). We will assume that at $x = \infty$ all the quantities ($\varphi(x)$, $\mathcal{T}(x)$ and $\mathcal{M}(x)$) are zero and thus only the lower boundary ($x = 0$) will contribute to the solution of (B.7).

For a DCB with prescribed displacements, the boundary conditions at the crack tip read

$$w(0) = \delta_c/2; \quad \varphi(0) = \theta_c; \quad \mathcal{M}(0) = F \cdot a; \quad \mathcal{T}(0) = F; \tag{B.8}$$

where by θ_c we denote the cross-sectional rotation of the arm at the crack tip. Applying the boundary conditions (B.8)–(B.7) gives

$$\Omega = \frac{F^2 a^2}{bEI} + \frac{F^2}{b\mu A_s} - \frac{2F\theta_c}{b}, \tag{B.9}$$

where the first term is the typical solution from LEFM where rotation of the crack tip is not taken into account, the second term represents the contribution of the shear strains and the third term is the influence of the rotation at the crack tip. Since for an Euler–Bernoulli or Timoshenko cantilever beam $\theta_v = \theta_c - Fa^2/(2EI)$, where θ_v is the rotation of the cross section at the point of the application of the force F, the final result (B.9) can be also written as

$$\Omega = \frac{F^2}{b}\left(\frac{1}{\mu A_s} - \frac{2\theta_v}{F}\right). \tag{B.10}$$

Note that this expression is equivalent to Eq. (A.5) for J_c^T which demonstrates that in case of a homogeneous interface $J_c^T = \Omega$. If the shear strains are neglected we obtain the expression

$$\Omega = -\frac{2F\theta_v}{b} \tag{B.11}$$

which is the same expression as J_c^E in Eq. (53) and has been reported by a number of authors in the literature (Paris and Paris, 1988; Högberg et al., 2007; Biel and Stigh, 2008; Zhu et al., 2009).

The boundary conditions for a DCB with prescribed rotations read

$$w(0) = \delta_c/2; \quad \varphi(0) = \theta_c; \quad \mathcal{M}(0) = M; \quad \mathcal{T}(0) = 0; \tag{B.12}$$

which applied to Eq. (B.7) give

$$\Omega = \frac{M^2}{bEI}. \tag{B.13}$$

This expression confirms once again that LEFM definition for G_c (see Eq. (52)) is equivalent to Ω for any length of cohesive zone as long as crack propagation is steady state. Again, expression (B.13) is in accordance with the J-integral solution proposed in the literature (Rice, 1968b; Suo et al., 1992; Sørensen et al., 1996; Lindhagen and Berglund, 2000).

It is worth remembering that formulae (B.10), (B.11) and (B.13) have been obtained for the case of a homogeneous interface, on which the traction-separation law is the same for each point of the interface. If the traction-separation law changes along the interface, these formulae cease to be valid, regardless of whether they are obtained through the procedure reported here or by computing the J integral. Numerical results confirming this theoretical finding are reported in Section 4.4.

Appendix C. Limit values for G_c^T and $\mathrm{d}a_{eqT}/\mathrm{d}a$ in the case of a brittle crack ($\sigma_{max} = \infty$)

By combining expressions (36) and (37), after solving a cubic equation, we can express a_{eqT} in terms of a_{eqE} as

$$a_{eqT} = \sqrt[3]{\chi} - \eta\sqrt[3]{\frac{1}{\chi}}, \tag{C.1}$$

where

$$\chi = \frac{a_{eqE}^3}{2} + \sqrt{\frac{a_{eqE}^6}{4} + \eta^3} \tag{C.2}$$

and $\eta = EI/\mu A_s$. It can be easily shown that as $\mu A_s \to \infty$, in the limit $\eta = 0$, $\chi = a_{eqE}^3$ and $a_{eqT} = a_{eqE}$. By combining Eq. (45) we can obtain

$$\frac{G_c^T}{G_c^E} = \frac{a_{eqT}^2 + \eta}{a_{eqE}^2}, \tag{C.3}$$

which using (C.1) becomes

$$\frac{G_c^T}{G_c^E} = \frac{\chi^{\frac{2}{3}} - \eta + \eta^2\chi^{-\frac{2}{3}}}{a_{eqE}^2}. \tag{C.4}$$

As expected, $\eta = 0$ in Eq. (C.4) returns $G_c^T = G_c^E$. Finally, from Eq. (C.1) we can obtain

$$\frac{\mathrm{d}a_{eqT}}{\mathrm{d}a_{eqE}} = \frac{\chi^{-\frac{2}{3}}}{3}\left(1 + \eta\ \chi^{-\frac{2}{3}}\right)\frac{\mathrm{d}\chi}{\mathrm{d}a_{eqE}}, \tag{C.5}$$

where

$$\frac{\mathrm{d}\chi}{\mathrm{d}a_{eqE}} = \frac{3}{2}a_{eqE}^2\left(1 + \frac{a_{eqE}^3}{\sqrt{a_{eqE}^6 + 4\eta^3}}\right). \tag{C.6}$$

Again, we can show that for $\eta = 0$, $\mathrm{d}\chi/\mathrm{d}a_{eqE} = 3\ a_{eqE}^2$ and $\mathrm{d}a_{eqT}/\mathrm{d}a_{eqE} = 1$.

As already mentioned, in the case of infinitely stiff interface $G_c^E = \Omega$ and $a = a_{eqE}$ and thus expressions (C.4) and (C.5) can be used to define limit values for G_c^T/Ω and $\mathrm{d}a_{eqT}/\mathrm{d}a$ when $\sigma_{max} = \infty$. These limit values are presented graphically in Fig. 7.

References

Alfano, G., Crisfield, M.A., 2001. Finite element interface models for the delamination analysis of laminated composites: mechanical and computational issues. Int. J. Numer. Methods Eng. 50 (7), 1701–1736.

Alfano, M., Furgiuele, F., Pagnotta, L., Paulino, G., 2011. Analysis of fracture in aluminum joints bonded with a bi-component epoxy adhesive. J. Test. Eval. 39 (2), 1–8.

Anderson, T.L., 1995. Fracture Mechanics – Fundamentals and Applications, 2nd ed. CRC Press.

ASTM D3433-99(2012). Standard Test Method for Fracture Strength in Cleavage of Adhesives in Bonded Metal Joints. ASTM International, 2012.

ASTM D5528 - 13. Standard Test Method for Mode I Interlaminar Fracture Toughness of Unidirectional Fiber-reinforced Polymer Matrix Composites. ASTM International, 2013.

Banea, M., da Silva, L., Campilho, R., 2010. Temperature dependence of the fracture toughness of adhesively bonded joints. J. Adhes. Sci. Technol. 24, 2011–2026.

Biel, A., Stigh, U., 2007. An analysis of the evaluation of the fracture energy using the DCB-specimen. Arch. Mech. 59 (4-5), 311–327.

Biel, A., Stigh, U., 2008. Effects of constitutive parameters on the accuracy of measured fracture energy using the DCB-specimen. Eng. Fract. Mech. 75, 2968–2983.

Blackman, B.R.K., Hadavinia, H., Kinloch, A.J., Williams, J.G., 2003a. The use of a cohesive zone model to study the fracture of fibre composites and adhesively-bonded joints. Int. J. Fract. 119, 25–46.

Blackman, B. R. K., Kinloch, A. J., 1997. Determination of the mode I adhesive fracture energy, G_{IC}, of structural adhesives using the double cantilever beam (DCB) and the tapered double cantilever beam (TDCB) specimens. ESIS TC4 ProtocolVersion 97-04.

Blackman, B.R.K., Kinloch, A.J., Paraschi, M., Teo, W.S., 2003b. Measuring the mode I adhesive fracture energy, G_{IC}, of structural adhesive joints: the results of an international round-robin. Int. J. Adhes. Adhes. 23, 293–305.

BS ISO 15024:2001, Fibre-reinforced Plastic Composites – Determination of Mode I Interlaminar Fracture Toughness, G_{Ic}, for Unidirectionally Reinforced Materials. British Standard, 2001.

BS ISO 25217:2009, Adhesives – Determination of the Mode I Adhesive Fracture Energy of Structural Adhesive Joints Using Double Cantilever Beam and Tapered Double Cantilever Beam Specimens. British Standard, 2009.

Campilho, R., Moura, D., Banea, M., da Silva, L., 2015. Adhesive thickness effects of a ductile adhesive by optical measurement techniques. Int. J. Adhes. Adhes. 57, 125–132.

Dimitri, R., Cornetti, P., Mantič, V., Trullo, M., De Lorenzis, L., 2017. Mode-I debonding of a double cantilever beam: a comparison between cohesive crack modeling and finite fracture mechanics. Int. J. Solids Struct. 124, 57–72.

Freiman, S.W., Mulville, D.R., Mast, P.W., 1973. Crack propagation studies in brittle materials. J. Mater. Sci. 8, 1527–1533.

Högberg, J.L., Sørensen, B.F., Stigh, U., 2007. Constitutive behaviour of mixed mode loaded adhesive layer. Int. J. Solids Struct. 44, 8335–8354.

Lemaitre, J., Chaboche, J., 1990. Mechanics of Solid Materials. University Press, Cambridge.

Lindhagen, J.E., Berglund, L.A., 2000. Application of bridging-law concepts to short–fibre composites. Part 1: DCB test procedures for bridging law and fracture energy. Compos. Sci. Technol. 60, 871–883.

Lopes, R.M., Campilho, R.D.S.G., da Silva, F.J.G., Faneco, T.M.S., 2016. Comparative evaluation of the double-cantilever beam and tapered double-cantilever beam tests for estimation of the tensile fracture toughness of adhesive joints. Int. J. Adhes. Adhes. 67, 103–111.

de Moura, M.F.S.F., Campilho, R.D.S.G., Gonçalves, J.P.M., 2008. Crack equivalent concept applied to the fracture characterization of bonded joints under pure mode I loading. Compos. Sci. Technol. 68, 2224–2230.

Olsson, P., Stigh, U., 1989. On the determination of the constitutive properties of thin interphase layers – an exact inverse solution. Int. J. Fract. 41, R71–R76.

Holoborodko, P., 2017. Applied Mathematics and Beyond – Central Differences. http://www.holoborodko.com/pavel/numerical-methods/numerical-derivative/central-differences/.

Paris, A.J., Paris, P.C., 1988. Instantaneous evaluation of J and C*. Int. J. Fract. 38, R19–R21.

Rice, J., 1968a. Mathematical analysis in the mechanics of fracture. In: Liebowitz, H. (Ed.), Fracture: An Advance Treatise (Vol. 2, Mathematical Fundamentals). Academic Press, N.Y., pp. 191–311.

Rice, J.R., 1968b. A path independent integral and the approximate analysis of strain concentration by notches and cracks. J. Appl. Mech. 35, 379–386.

Ripling, E.J., Mostovoy, S., Corten, H.T., 1971. Fracture mechanics: a tool for evaluating structural adhesives. J. Adhes. 3 (2), 107–123.

Ripling, E. J., Mostovoy, S., Patrick, R. L., 1964. Measuring Fracture Toughness of Adhesive Joints. Materials Research and Standards (ASTM) 64 (3), 129–134.

Sarrado, C., Turon, A., Costa, J., Renart, J., 2016. On the validity of linear elastic fracture mechanics methods to measure the fracture toughness of adhesive joints. Int. J. Solids Struct. 81, 110–116.

Sørensen, B.F., 2002. Cohesive law and notch sensitivity of adhesive joints. Acta Mater. 50, 1053–1061.

Sørensen, B.F., Brethe, P., Skov-Hansen, P., 1996. Controlled crack growth in ceramics: the DCB specimen loaded with pure moments. J. Eur. Ceram. Soc. 16, 1021–1025.

Sørensen, B.F., Jacobsen, T.K., 2003. Determination of cohesive laws by the J integral approach. Eng. Fract. Mech. 70, 1841–1858.

Suo, Z., Bao, G., Fan, B., 1992. Delamination R-curve phenomena due to damage. J. Mech. Phys. Solids 40 (1), 1–16.

Tamuz, V., Tarasovs, S., Vilks, U., 2003. Delamination properties of translaminar-reinforced composites. Compos. Sci. Technol. 63, 1423–1431.

Turon, A., Davila, C., Camanho, P., Costa, J., 2007. An engineering solution for mesh size effects in the simulation of delamination using cohesive zone models. Eng. Fract. Mech. 74, 1665–1682.

Škec, L., Jelenić, G., 2017. Geometrically non-linear multi-layer beam with interconnection allowing for mixed-mode delamination. Eng. Fract. Mech. 169, 1–17.

Škec, L., Jelenić, G., Lustig, N., 2015. Mixed-mode delamination in 2D layered beam finite elements. Int. J. Numer. Methods Eng. 104, 767–788.

Zhao, Y., Seah, L., Chai, G., 2016. Measurement of interlaminar fracture properties of composites using the J-integral method. J. Reinf. Plast. Compos. 35 (14), 1143–1154.

Zhu, Y., Liechti, K.M., Ravi-Chandar, K., 2009. Direct extraction of rate-dependent traction-separation laws for polyurea/steel interfaces. Int. J. Solids Struct. 46, 31–51.